Atmospheric
Chemistry
and Physics

Long-term trends of surface ozone and its influencing factors at the Mt Waliguan GAW station, China – Part 2: The roles of anthropogenic emissions and climate variability

Wanyun Xu[1], Xiaobin Xu[1], Meiyun Lin[2], Weili Lin[3], David Tarasick[4], Jie Tang[5], Jianzhong Ma[1], and Xiangdong Zheng[1]

[1]State Key Laboratory of Severe Weather & Key Laboratory for Atmospheric Chemistry,
Institute of Atmospheric Composition, Chinese Academy of Meteorological Sciences,
Beijing, 100081, China
[2]NOAA Geophysical Fluid Dynamics Laboratory and Program in Atmospheric and Oceanic Sciences in Princeton University,
Princeton, New Jersey 08540, USA
[3]College of Life and Environmental Sciences, Minzu University of China, Beijing, 100081, China
[4]Science and Technology Branch, Environment and Climate Change Canada, 4905 Dufferin Street,
Downsview, Ontario, M3H 5T3, Canada
[5]Meteorological Observation Center, China Meteorological Administration, Beijing, 100081, China

Correspondence: Xiaobin Xu (xuxb@camscma.cn)

Abstract. Inter-annual variability and long-term trends in tropospheric ozone are both environmental and climate concerns. Ozone measured at Mt Waliguan Observatory (WLG, 3816 m a.s.l.) on the Tibetan Plateau over the period of 1994–2013 has increased significantly by 0.2–0.3 ppbv yr^{-1} during spring and autumn but shows a much smaller trend in winter and no significant trend in summer. Here we explore the factors driving the observed ozone changes at WLG using backward trajectory analysis, chemistry–climate model hindcast simulations (GFDL AM3), a trajectory-mapped ozonesonde data set, and several climate indices. A stratospheric ozone tracer implemented in GFDL AM3 indicates that stratosphere-to-troposphere transport (STT) can explain $\sim 60\%$ of the simulated springtime ozone increase at WLG, consistent with an increase in the NW air-mass frequency inferred from the trajectory analysis. Enhanced STT associated with the strengthening of the mid-latitude jet stream contributes to the observed high ozone anomalies at WLG during the springs of 1999 and 2012. During autumn, observations at WLG are more heavily influenced by polluted air masses originating from South East Asia than in the other seasons. Rising Asian anthropogenic emissions of ozone precursors are the key driver of increasing autumnal ozone observed at WLG, as supported by the GFDL AM3 model with time-varying emissions, which captures the observed ozone increase (0.26 ± 0.11 ppbv yr^{-1}). AM3 simulates a greater ozone increase of 0.38 ± 0.11 ppbv yr^{-1} at WLG in autumn under conditions with strong transport from South East Asia and shows no significant ozone trend in autumn when anthropogenic emissions are held constant in time. During summer, WLG is mostly influenced by easterly air masses, but these trajectories do not extend to the polluted regions of eastern China and have decreased significantly over the last 2 decades, which likely explains why summertime ozone measured at WLG shows no significant trend despite ozone increases in eastern China. Analysis of the Trajectory-mapped Ozonesonde data set for the Stratosphere and Troposphere (TOST) and trajectory residence time reveals increases in direct ozone transport from the eastern sector during autumn, which adds to the autumnal ozone increase. We further examine the links of ozone variability at WLG to the quasi-biennial oscillation (QBO), the East Asian summer monsoon (EASM), and the sunspot cycle. Our results suggest that the 2–3-, 3–7-, and 11-year periodicities are linked to the QBO, EASM index, and sunspot cycle, respectively. A multivariate regression analysis is performed to quantify the relative

contributions of various factors to surface ozone concentrations at WLG. Through an observational and modelling analysis, this study demonstrates the complex relationships between surface ozone at remote locations and its dynamical and chemical influencing factors.

1 Introduction

Ozone in the troposphere is a potent greenhouse gas, an air pollutant detrimental to human health and vegetation, and the primary source of hydroxyl radicals, which play a critical role in atmospheric chemistry. The long-term variation in ozone is of both environmental and climate concern. Therefore, it is important to trace the long-term variations in ozone at different locations and understand the causes of such variations. Continuous long-term observations of surface ozone have only been made at a few representative sites in China. The Mt Waliguan (WLG) station (36°17′ N, 100°54′ E, 3816 m a.s.l.), established in 1994, is situated in the northeastern part of the Tibetan Plateau, where population is sparse and industries hardly exist. It is one of the baseline stations in the Global Atmosphere Watch (GAW) program of the World Meteorological Organization (WMO) and the only one in the hinterland of the Eurasian continent with surface ozone measurement of longer than 2 decades. The long-term trend and periodicity of surface ozone at WLG during 1994–2013 are reported in the companion paper (Xu et al., 2016). Significant increasing trends have been detected in spring and autumn, while observations show no significant trend during summer when ozone is at its seasonal maximum. Here we investigate the mechanisms controlling the seasonal ozone trends measured at WLG using backward trajectory analysis and multi-decadal hindcast simulations (1980–2014) conducted with the Geophysical Fluid Dynamics Laboratory chemistry–climate model (Lin et al., 2014, 2015a, 2017).

With rapid economic development in eastern China, anthropogenic emissions of ozone precursors have been increasing during the past 2 decades (van der A et al., 2006; Kurokawa et al., 2013; Itahashi et al., 2014). Specifically, emissions of NO_x over eastern China have tripled since 1990 (e.g. Lin et al., 2017). Increasing levels of surface and free tropospheric ozone have been detected at several locations in eastern China, e.g. in the North China Plain (Ding et al., 2008; Wang et al., 2012, 2017; Ma et al., 2016; Sun et al., 2016), the Yangtze River Delta (Xu et al., 2008), and the Pearl River Delta (Wang et al., 2009; Lin et al., 2017). Rising Asian anthropogenic emissions of ozone precursors have been implicated in raising free tropospheric and surface ozone levels over the western US during spring (Verstraeten et al., 2015; Lin et al., 2015b, 2017). A recent study by Lin et al. (2017) shows that a tripling of NO_x emissions in Asia contributed up to 50–65 % of the observed spring-

time ozone increases at rural western US sites during 1988–2014, outpacing ozone decreases resulting from US domestic NO_x emission controls. A few case studies have documented the influence of anthropogenic pollution from eastern and central China on ozone at WLG during the summer season (Wang et al., 2006b; Xue et al., 2011), but whether the growth in East Asian anthropogenic ozone precursor emissions has contributed to the long-term trend of surface ozone at WLG has not yet been examined.

Aside from regional precursor emissions and long-range horizontal transport (Wang et al., 2006a; Lal et al., 2014), the concentration of surface ozone has many other influencing factors. For instance, surface ozone concentrations at high-elevation sites can also be increased by the downward transport of ozone-rich air from the stratosphere during deep convection and stratosphere-to-troposphere exchange (STE) events (Bonasoni et al., 2000; Stohl et al., 2000; Lefohn et al., 2012; Jia et al., 2015; Ma et al., 2014; Langford et al., 2009, 2015; Lin et al., 2012a, 2015a). Studies based on short-term measurements suggested that surface ozone at WLG is influenced by STE events in spring (Zheng et al., 2011) and sometimes during summer (Ding and Wang, 2006). The extent to which STE influences observed year-to-year variability and the decadal trend of ozone at WLG has not been previously investigated.

Changes in large-scale atmospheric circulation patterns can modulate long-range transport of ozone pollution in the troposphere as well as STE. Large-scale physical and dynamical processes including the El Niño–Southern Oscillation (ENSO), the North Atlantic Oscillation (NAO), the quasi-biannual oscillation (QBO), and the solar cycle (Creilson et al., 2003; Ziemke et al., 2005; Oman et al., 2013; Sioris et al., 2014) have been found to significantly affect stratospheric and tropospheric ozone variability. Based on the good correlation between the ENSO index and tropospheric column ozone (TCO) over tropical latitudes, Ziemke et al. (2010) created a so-called "Ozone ENSO Index" (OEI). Over northern mid-latitudes, strong El Niño events enhance long-range transport of Asian ozone pollution towards the eastern North Pacific and the southwestern US by modulating the strength and position of the subtropical jet stream (Lin et al., 2014). Some studies (Zeng and Pyle, 2005; Langford, 1999; Koumoutsaris et al., 2008; Voulgarakis et al., 2011) suggest that the change in dynamics after El Niño events can promote cross-tropopause ozone exchange and lead to a rise in global mean tropospheric ozone burden. However, Lin et al. (2015a) find that El Niño events lead to enhancements in upper tropospheric ozone but this influence does not reach surface air. Over high-elevation regions prone to deep stratospheric intrusions in the western US, Lin et al. (2015b) find that the increased frequency of deep tropopause folds that form in upper-level frontal zones following strong La Niña winters exerts a stronger influence on springtime ozone levels at the surface than the El Niño-related increase in lower stratospheric to upper tropospheric ozone burden.

Similar to the western US, the Tibetan Plateau has been identified as a preferred region for deep stratospheric intrusions (Škerlak et al., 2014). Prior studies show that the QBO, ENSO, and sunspot cycle influence total ozone over the Tibetan Plateau (Ji et al., 2001; Huang et al., 2009; Ningombam, 2011; Zou et al., 2001). The mechanisms controlling the inter-annual variability in jet stream characteristics, STE, and their influences on lower tropospheric ozone measured at WLG are poorly characterised. In addition, China is strongly influenced by the East Asian summer monsoon (EASM). Past studies have pointed out that the EASM influences ozone concentrations in this region through altering the transport of anthropogenic pollution (Derong et al., 2013; Liu et al., 2009, 2011). Using the GEOS-Chem global chemical transport model, Yang et al. (2014) report a positive inter-annual correlation between the EASM and the Tibetan surface ozone concentration. Their results were not evaluated with actual observations of surface ozone.

In this work, we aim to advance knowledge on the factors driving inter-annual variability and long-term trends in ozone at WLG over the past 3 decades. Section 2 briefly describes observational data, model simulations, and the analysis approach. In Sect. 3, we first discuss the links of surface ozone at WLG to air-mass origin, including their seasonal to inter-annual variability (Sect. 3.1). We then use the GFDL AM3 model hindcast simulations to interpret the influences of changes in meteorology, STE, and anthropogenic emissions on ozone measured at WLG in winter, spring, summer, and autumn (Sect. 3.2) and the impact of direct ozone transport versus precursor transport (Sect. 3.3). Section 4 examines the relationship between atmospheric dynamics and surface ozone at WLG, including the influence of STE, EASM, and the sunspot cycle. An empirical model is obtained for the normalised monthly level of surface ozone at WLG using the multivariate regression technique and is used to explain the observed ozone trends.

2 Data and methodology

2.1 Data

Ozone concentration and meteorological parameters were measured at the WLG site (36°17′ N, 100°54′ E, 3816 m a.s.l.) in Qinghai Province, China. Ozone concentrations at a 5 min resolution from August 1994 to December 2013 were averaged into hourly, daily, and monthly timescales, with a data completeness of 75 % required for each averaging step. Hilbert–Huang transform (HHT) analysis was performed using the monthly average daytime and nighttime ozone data. Further details on the site, measurements, daytime and nighttime data subsets, and HHT calculations can be found in Part 1 of our study (Xu et al., 2016). In this paper, the results of the HHT analysis are further associated with the sunspot number (SSN), QBO,

and EASM index (Li and Zeng, 2002) to investigate the influence of various climate oscillations on surface ozone at WLG. The SSN data are from Sunspot Index and Long-term Solar Observations (http://www.sidc.be/silso/datafiles). The QBO index is based on the 30 hPa Singapore zonal wind and available from the US National Oceanic and Atmospheric Administration at https://www.esrl.noaa.gov/psd/data/climateindices/. The EASM index is acquired from http://ljp.gcess.cn/dct/page/65577. We also use monthly CO data based on weekly flask sampling at 5 m above ground, obtained from the World Data Centre for Greenhouse Gases (http://ds.data.jma.go.jp/gmd/wdcgg/wdcgg.html), to infer changes of regional emissions near WLG. Using high-frequency (e.g. minutes) in situ observations of CO and water vapour would be ideal to diagnose the presence of stratospheric versus anthropogenic influences; however, continuous high-quality data are not available at WLG due to various technical challenges.

2.2 Backward trajectory analysis

The HYSPLIT model (version 4) from NOAA Air Resources Laboratory (Draxler and Hess, 1997, 1998; Draxler, 1999) is used for the trajectory analyses, using three different meteorological data sets from NCEP. The NCEP Global Reanalysis Data with a spatial resolution of 2.5°, the NCEP FNL operational data in 1.0° resolution, and the NCEP GDAS (Global Data Assimilation System) operational forecast data in 1.0° resolution are used for 1994–1996, 1997–2006, and 2007–2013, respectively. All the meteorology data have a temporal resolution of 6 h. The trajectory endpoint is set to 36.28° N and 100.90° E with a height of 100 m above the ground level. The 168 h (7 days) backward trajectories are calculated at a 6 h interval from 1 August 1994 to 31 December 2013.

To study the overall air-mass origin and to determine whether the air mass collected pollutants from nearby cities, the average direction of each trajectory relative to the WLG station is calculated for both the 168 h and 24 h trajectories (Fig. S1 in the Supplement). The 168 and 24 h average directions relative to WLG are clustered into bins of 45° and the occurrence frequency in each bin is calculated.

Since ozone is a trace gas with a distinct vertical distribution, it is not enough to just determine the direction from which the air mass came. The height of the air mass is also crucial for interpreting the measured ozone concentrations. As discussed in previous studies (Ma et al., 2002; Xu et al., 2016), the WLG site is predominantly influenced by air from the planetary boundary layer (PBL) during daytime and from the free troposphere (FT) during nighttime, with ozone concentrations showing a daytime minimum and a nighttime maximum. Daytime and nighttime ozone at WLG show different trends, particularly in summer (0.07 ± 0.18 ppb yr^{-1} for daytime and 0.22 ± 0.20 ppb yr^{-1} for nighttime; Xu et al., 2016). To investigate the impacts of air masses from the PBL and FT separately, the PBL height from the NCEP data,

which can be added in the HYSPLIT model along the trajectories, is used to judge whether the air mass that arrived at WLG represents the PBL or the FT. PBL trajectory sections are defined as the part of the trajectory that was continuously within the PBL before arriving at the station. Thus, PBL trajectory sections are usually close to the station. When the trajectory height exceeds that of the PBL, the rest of the trajectory is taken as the FT trajectory section. FT trajectory sections can also be close to the station, representing subsiding air from the FT near the station; however, most of them are located far away from the station.

2.3 Potential source contribution function analysis

The potential sources of high ozone are studied using the potential source contribution function (PSCF) analysis method, which has been widely applied to detect possible source regions (Ara Begum et al., 2005; Lucey et al., 2001; Zhou et al., 2004). The PSCF analysis is performed both on PBL and on FT trajectories to detect differences in source region distributions in the PBL and in the FT or above.

The PSCF on the grid (i, j) is defined as

$$PSCF = m(i, j)/n(i, j), \tag{1}$$

where $n(i, j)$ is the residence time of all the trajectories and $m(i, j)$ is the residence time of a subset of trajectories in the grid cell (i, j). Each trajectory is associated with ozone concentrations that were measured at its arrival time. The 75th percentile of all the ozone concentrations at WLG is calculated and the residence time in each grid cell $m(i, j)$ of the subset of trajectories that is associated with ozone concentration higher than the 75th percentile value is counted.

Abnormally high PSCF values may be produced for certain grid cells with small $n(i, j)$ values, which would bear large uncertainties. To avoid such uncertainties, a weighting factor $W(n_{ij})$ is introduced, which was originally proposed by Zeng and Hopke (1989):

$$W(n_{ij}) = \begin{cases} 1.0, & n_{ij} > \overline{n_{ij}} \\ 0.7, & 0.1 \cdot \overline{n_{ij}} < n_{ij} \le \overline{n_{ij}} \\ 0.4, & 0.05 \cdot \overline{n_{ij}} < n_{ij} \le 0.1 \cdot \overline{n_{ij}} \\ 0.2, & n_{ij} \ge 0.05 \cdot \overline{n_{ij}} \end{cases}, \tag{2}$$

where $\overline{n_{ij}}$ is the average number of n_{ij}.

2.4 Calculation of direct ozone transport contribution

A Trajectory-mapped Ozonesonde data set for the Stratosphere and Troposphere (TOST) was generated from the ozone sounding records with trajectory mapping by Liu et al. (2013). The data set has a spatial resolution of $5° \times 5° \times 1\,\mathrm{km}$ (latitude, longitude, and altitude). A subset from the TOST, the global three-dimensional (3-D) monthly average tropospheric ozone from 1994 to 2012 is applied in this paper to calculate the contribution of direct tropospheric

ozone transport to the ozone trends at WLG. The 3-D tropospheric ozone data are in monthly intervals. A 3-D backward trajectory residence time within the same grids and with the same time interval as that of the tropospheric ozone data is calculated based on the backward trajectory analysis results in Sect. 2.3. Assuming that ozone is nearly conserved on the transport pathway (i.e. ozone and production and loss are negligible), the contribution of O_3 in each grid cell to the grid cell of WLG during each month is calculated using the trajectory residence time as a weighting factor:

$$O_{3,\,\mathrm{contrib}}(t, i) = \frac{O_3(t, i) \times T(t, i)}{\sum\limits_{i=1}^{n} T(t, i)}, \tag{3}$$

where $O_3(t, i)$ and $T(t, i)$ stand for the ozone concentration and the trajectory residence time, respectively, at time t in grid cell i, while n stands for the total number of grid cells.

To obtain the monthly time series of total direct tropospheric ozone transport contribution to ozone at WLG, the 3-D ozone contribution climatology of all the grid cells is summed up (Eq. 4). The bottom layer of the grid cell in which WLG resides is excluded from the summation.

$$O_{3,\,\mathrm{contrib,\,tot}} = \sum\limits_{i=1}^{n} O_{3,\,\mathrm{contrib}}(t, i) \tag{4}$$

The variation trend of $O_{3,\,\mathrm{contrib}}(t, i)$ and $O_{3,\,\mathrm{contrib,\,tot}}$ is calculated for the entire period of 1994–2013 and separately for each season. For display, $O_{3,\,\mathrm{contrib}}(t, i)$ and its trend is integrated over height. $O_{3,\,\mathrm{contrib,\,tot}}$ is used in the multivariate regression as $O_{3,\,\mathrm{trop}}$ in Sect. 2.6.

2.5 Modelling of stratospheric and anthropogenic contributions

The GFDL AM3 global chemistry–climate model was used to make hindcast simulations of ozone and related tracers at $\sim 200 \times 200\,\mathrm{km}^2$ horizontal resolution over the 1980–2014 period (Lin et al., 2015a, b, 2014, 2017). The model is nudged to the NCEP/NCAR reanalysis zonal and meridional winds using a pressure-dependent nudging technique (Lin et al., 2012b). Two AM3 simulations are used in this study: one with both meteorology and anthropogenic emissions varying from 1980 to 2014 (BASE) and the other with anthropogenic emissions (including methane) held constant in time (FIXEMIS). To quantify the stratospheric influence on surface ozone, a stratospheric ozone tracer (O_3Strat) is defined relative to a dynamically varying tropopause and is subjected to chemical and depositional loss in the same manner as odd oxygen of tropospheric origin (Lin et al., 2015a). Carbon-monoxide-like tracers for East Asia (EACOt), Europe (EUCOt), and North America (NACOt) are implemented to investigate the impact of circulation changes on hemispheric pollution transport (Lin et al., 2014).These CO-like tracers have a 50-day exponential lifetime and are simulated with

surface emissions held constant in time from each of the three northern mid-latitude source regions. Comparison with available observations from the mid-1990s to the 2000s at a suite of sites across Asia shows that GFDL AM3 captures 65–90 % of the observed ozone increases in Asia (Lin et al., 2017). The long-term ozone observational record at WLG provides an important test for the GFDL AM3 model to represent the key processes driving year-to-year variability and trends in tropospheric ozone in the remote atmosphere of the Tibetan Plateau. For comparison with measurements at the 3.8 km altitude of WLG, the model is sampled at the grid box containing WLG and at the 700 hPa layer. This approach is appropriate because observations at WLG are representative of large-scale conditions with little influence from local urban emissions.

2.6 Multivariate regression of surface ozone at Waliguan

Multivariate regression is applied to obtain an empirical model to explain the relationship and contribution of the various influencing factors to the surface ozone concentration at WLG. The regression model takes on the following form:

$$O_3 = \alpha(t) + \sum_{i=1}^{n} \beta_i(t) \cdot \text{factor}_i(t), \tag{5}$$

where $\alpha(t)$ is a third-order harmonic function used to interpret the background variation signal of surface ozone:

$$\alpha(t) = a_0 + \sum_{j=1}^{3} a_{1,j} \cdot \cos(2\pi j(t - t_0)) + a_{2,j}$$
$$\cdot \sin(2\pi j(t - t_0)), \tag{6}$$

and $\sum_{i=1}^{n} \beta_i(t) \cdot \text{factor}_i(t)$ stands for the total contribution of the n-influencing factors used in the regression model. $\beta_i(t)$ is a first-order harmonic function, which can be expressed as

$$\beta_i(t) = b_{i,0} + b_{i,1} \cdot \cos(2\pi(t - t_0)) + b_{i,2}$$
$$\cdot \sin(2\pi(t - t_0)). \tag{7}$$

The coefficients $b_{i,1}$ and $b_{i,2}$ allow for the time-dependent intensification or attenuation of the influences of factors. Since our data start in the year of 1994, t is calculated as

$$t = \text{year} + (\text{month} - 1)/12 - 1994. \tag{8}$$

3 Key drivers of long-term ozone trends at WLG

3.1 Climatology and inter-annual variability in air-mass origin at WLG

Based on past studies, which were mostly focused on summertime ozone at WLG, high ozone concentrations were mostly linked to downward transport, instead of horizontal transport of anthropogenic pollution (Zhu et al., 2004; Ma et al., 2005; Wang et al., 2006b; Xue et al., 2011). Westerly trajectories were commonly associated with downward transport events and high ozone concentrations, whereas easterly trajectories carried air masses with signals of anthropogenic pollution and lower ozone concentrations. Anthropogenic impact was attributed mostly to the two big cities, Xining and Lanzhou, that are both located to the east of WLG; however, central and eastern China could also have potential impacts (Wang et al., 2006b; Xue et al., 2011).

Since ozone and its precursors are usually inhomogeneously distributed, both the horizontal direction and vertical height of the air-mass origin may influence the local concentration of ozone at WLG. As already pointed out in previous studies (Ma et al., 2002; Xu et al., 2016), during daytime and nighttime the WLG site is mainly influenced by air from the PBL and FT, respectively, causing a daytime minimum and a nighttime maximum of the ozone concentration. Furthermore, ozone in daytime and nighttime showed different trends, particularly in summer when daytime and nighttime ozone showed respective trends of 0.07 ± 0.18 and 0.22 ± 0.20 ppb yr^{-1} (Xu et al., 2016). To locate the origin of high surface ozone concentrations at WLG and understand the ozone difference between daytime and nighttime, it is necessary to investigate the respective impacts of air masses from the PBL and FT. To locate the origin of high surface ozone concentrations at WLG, a PSCF analysis (Sect. 2.3) was performed separately for the PBL and FT trajectories. Figure 1 displays the ozone PSCF of the PBL and FT trajectories in spring, summer, autumn, and winter from August 1994 to December 2013. For the PBL as well as the FT trajectories, the NW sector is most frequently accompanied by high ozone concentrations (higher than 75th percentile ozone concentration), which is a common phenomenon existing in all seasons.

During spring, Sichuan Province, which is southeast of WLG, displays a significantly high ozone PSCF both in the PBL and FT trajectories, which is possibly evidence for long-range transport of ozone and/or its precursors from Sichuan to WLG. During summer, when air masses from the east occur most frequently (as will be shown in Fig. 2), the entire eastern sector reveals low values of high ozone PSCF, hardly showing signs of anthropogenic influence on WLG. In other words, most air masses from the east in summer are not associated with high ozone. High ozone PSCF occurs dominantly with trajectories from the NW or N. In autumn, in addition to NW or N, significant contributions of trajectories from the E, SE, and S can also be discerned in the PBL trajectories, which suggests that high ozone is linked to air masses coming from western China, central China, the northeastern part of the Tibetan Plateau, the southwestern part of Gansu Province, and north of China (east Mongolia). In the FT trajectories, high ozone concentrations were mainly linked to air masses from western and central China. In addition, air
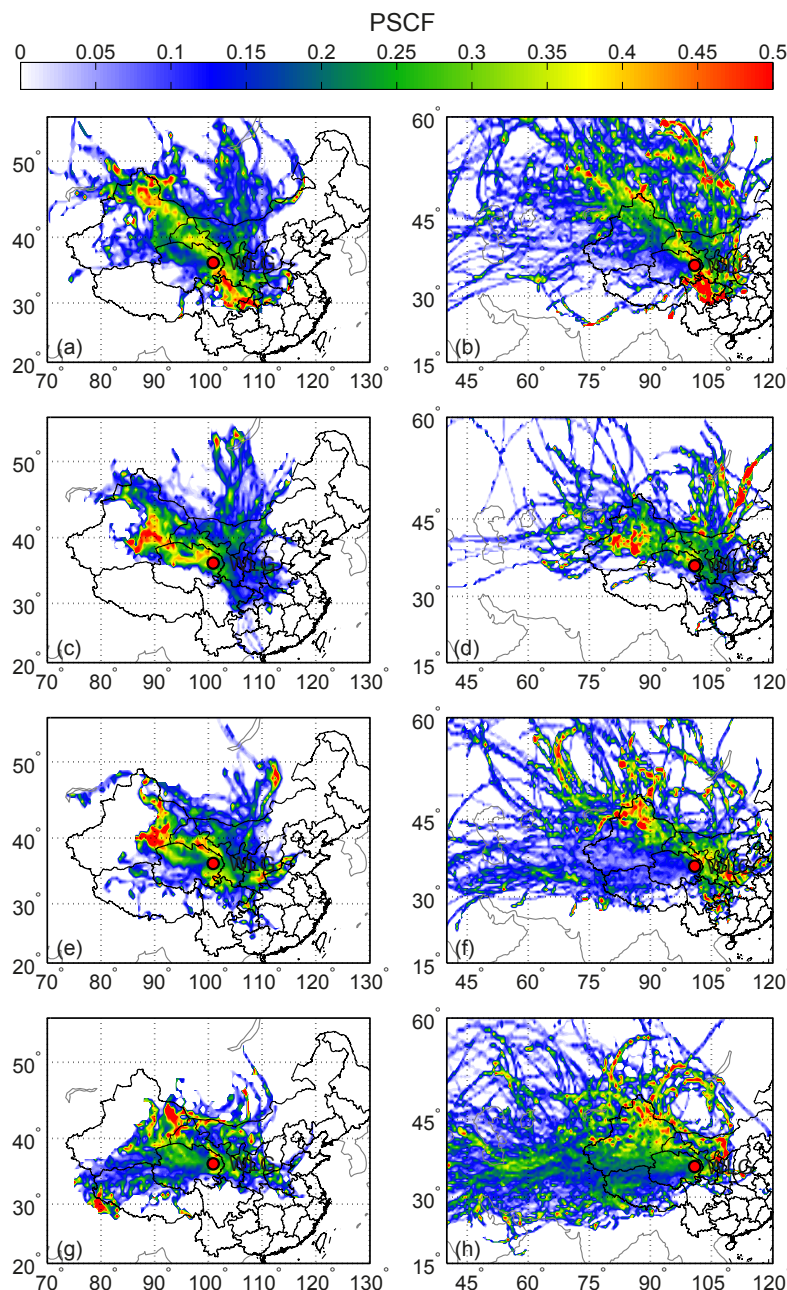
Figure 1. The 1994–2013 climatology of air-mass origins at WLG in the PBL **(a, c, e, g)** and FT **(b, d, f, h)** for spring **(a, b)**, summer **(c, d)**, autumn **(e, f)**, and winter **(g, h)** based on the PSCF analysis of ozone concentrations higher than the 75th percentile value (Sect. 2.3).

masses over Gansu Province, part of Sichuan Province, and some parts of Russia also show a high PSCF. In winter, the PBL trajectories show a high ozone PSCF mainly in the NW sectors; however, the SW and N-NE sectors also revealed scattered high PSCF values (over some parts of Nepal, northern India, Mongolia, and Inner Mongolia). Aside from the NW sector, the FT trajectories display a significantly high PSCF in the NE sector in the western half of Inner Mongolia.

To evaluate the impact of different air masses, we need to find out which air masses are influencing WLG and evaluate the relative importance of the different air masses during different seasons. Figure 2 depicts the 24 and 168 h average trajectory direction occurrence frequencies for spring, summer, autumn, and winter, respectively. The 168 h average trajectory direction provides us information on the overall origin of the air mass, while the 24 h average trajectory direction
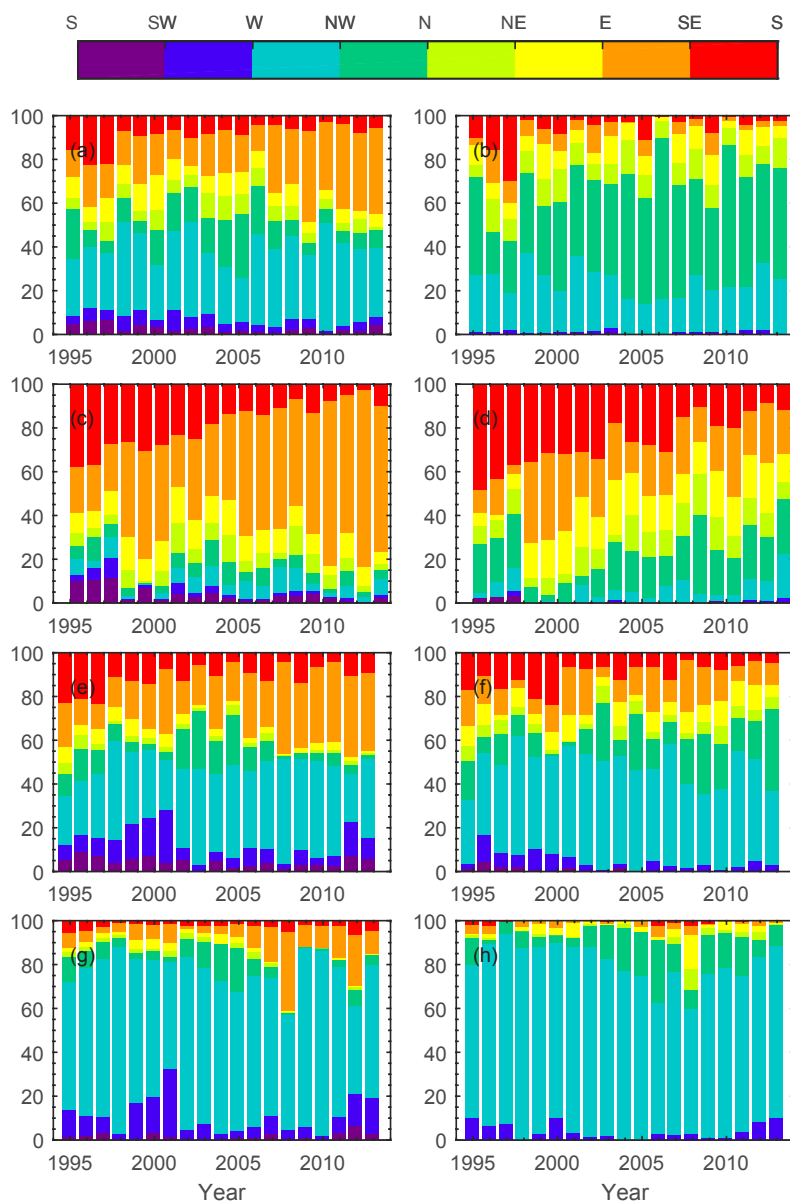
Figure 2. The average trajectory direction occurrence frequencies in **(a, b)** spring, **(c, d)** summer, **(e, f)** autumn, and **(g, h)** winter of **(a, c, e, g)** $t < 24$ h and **(b, d, f, h)** $t < 168$ h.

should be able to reveal if the air mass passed over nearby polluted regions before arriving at the station.

From the 168 h average trajectory direction occurrence frequencies (Fig. 2b, d, f, h), it can be seen that WLG is under the major influence of western and northwestern air masses throughout the year, with air masses from the east only playing a significant role during summer, which is in accordance with previous studies (e.g. Zhang et al., 2011). Hence, the WLG site is overall very clean and highly representative of a background state. Trajectories from the east (including the NE, E, and SE) take up on average 20, 65, 31, and 6 % of all the trajectory directions during spring, summer, autumn,

and winter, respectively. For $t = -168$ h, the NW trajectories are most frequent in spring (44 %) and least frequent in winter (12 %), while western trajectories are most dominant in winter (77 %) and least dominant in summer (6 %).

From the 168 h average trajectory direction frequencies, it can be seen that the anthropogenic influence is strongest in summer, followed by autumn, and is almost negligible in winter. However, the 24 h average trajectory direction frequencies show significantly larger portions of eastern trajectories and smaller percentages of northwestern trajectories (Fig. 2a, c, e, g), implying that a significant part of air masses originating from the northwest of WLG often bend over to

Table 1. The linear variation slope (k) of the 24 h and 168 h average trajectory direction occurrence frequencies (% yr^{-1}; numbers in bold are significant under a confidence level of 95 %).

k (% yr^{-1})	Season	Trajectory direction							
		S	SW	W	NW	N	NE	E	SE
$t \leq 24$ h	MAM	**−0.17**	**−0.19**	0.39	−0.32	−0.11	**−0.30**	**1.38**	**−0.69**
	JJA	**−0.42**	**−0.20**	0.04	−0.13	−0.01	−0.23	**2.75**	**−1.80**
	SON	−0.16	−0.24	0.60	−0.41	**−0.17**	**−0.32**	**1.39**	**−0.69**
	DJF	0.08	−0.17	−0.30	−0.22	**−0.09**	**−0.17**	**0.84**	0.05
$t \leq 168$ h	MAM	−0.01	0.01	−0.27	**1.34**	−0.01	−0.01	**−0.38**	**−0.67**
	JJA	**−0.10**	0.02	**0.42**	0.57	0.31	**0.50**	0.15	**−1.87**
	SON	**−0.14**	**−0.32**	0.05	**0.91**	0.03	0.13	0.04	**−0.71**
	DJF	0.01	−0.09	−0.67	0.54	0.17	0.11	−0.05	−0.02

the east 24 h before arriving at WLG. On average 24 h trajectories from the east (including the NE, E, and SE) take up 40, 76, 30, and 15 % of all the trajectory directions during spring, summer, autumn, and winter, respectively. Air-mass trajectories originating from the far northwest bending to the east before their arrival at WLG may entrain pollutants if they travel over the large cities. The large occurrence frequency of eastern trajectories in the endpoints within the last 24 h suggests that anthropogenic influences on WLG during spring and autumn should not be neglected.

It is also worth noting from Fig. 2 that the trajectory direction frequencies were far from constant throughout the 2 decades from 1994 to 2013. There was large inter-annual variability. Some directions show significant variation trends in their occurrence frequencies, which will be discussed later in this section.

The air-mass direction analysis shows that the WLG site is under the influence of different air masses from different horizontal directions. Apart from that, the WLG site is also under the control of distinct air masses from different layers throughout the day, with PBL air masses dominating during the day and FT air masses during the night, which led to a clear diurnal variation with high nighttime and low daytime ozone concentrations (Ma et al., 2002; Xu et al., 2016). STE events were also held responsible for the injection of stratospheric ozone into the troposphere, leading to elevated surface ozone concentrations (Bonasoni et al., 2000; Ding and Wang, 2006; Stohl et al., 2000; Tang et al., 2011; Lefohn et al., 2012; Jia et al., 2015; Ma et al., 2014; Lee et al., 2007; Liang et al., 2008).

Changes in atmospheric circulations might lead to variations in the occurrence frequencies of air masses from different directions shown in Fig. 2. Due to the high dependence of local surface ozone concentrations on the air-mass origin, a significant change in atmospheric circulation may lead to changing local concentrations of surface ozone at WLG. To investigate this kind of impact, average 24 h and 168 h trajectory directions are used to uncover whether there

were secular changes in the occurrence frequency of different directions. Table 1 lists the variation trends (k, slopes of linear regression) of trajectory direction occurrence frequencies in different seasons. The bold numbers in the table are the variation trends that are statistically significant ($p < 0.05$). From the 168 h results it can be noted that the NW trajectories gained frequency in the 2 decades between 1994 and 2013 and the increasing trend is statistically significant in spring (1.34 % yr^{-1}) and autumn (0.91 % yr^{-1}), which would amount to total increases of 26.8 and 18.2 % by the end of the 2 decades. As is discussed in the PSCF analysis, the NW trajectories are associated with high ozone concentrations during all seasons (Fig. 1) and thus an increase in their occurrence frequency would lead to an increase in surface ozone concentration at WLG. The SE trajectories are also often accompanied by high ozone concentrations, representing possible transport of ozone precursors that are from anthropogenic sources from Sichuan, southeastern China, and South East Asian countries to WLG. However, the SE trajectories have been significantly decreasing in spring, summer, and autumn, with the strongest decrease found in summer (−1.87 % yr^{-1}), suggesting that changes in air-mass origin alone cannot explain the seasonal ozone trends measured at WLG.

Table 1 shows an increasing trend in the occurrence frequency of E trajectories in the 24 h average directions but not in the 168 h average directions. This indicates that more trajectories from other directions were turning over to the east of WLG 24 h before their arrival at the site. During spring and autumn, only an increase in the 168 h NW trajectories was found, while during summer, increases were found in both the 168 h W and NE trajectories; these increases are highly possibly linked to the increase in 24 h E trajectories. The SE 24 h trajectories, however, show significant decreasing trends in spring, summer, and autumn, with the strongest decrease in summer. This is consistent with the 168 h results, suggesting that the entire SE air-mass transport pathway decreased in frequency.

Since the NW direction is often linked to high ozone concentrations according to the PSCF and a significant increase in 168 h trajectory occurrences from that direction has been detected, a more detailed examination on that part of the trajectories is necessary. Figure 3 displays the occurrence frequency of 168 h average trajectories in the NW sector that turned to the E, NW, and W sectors in the last 24 h, with the lines indicating the according decadal linear variation trends. It can be seen that more and more NW trajectories bent to the E sector before arriving at WLG, with significant trends in all seasons and the largest increasing slope in spring. The trajectories originating from the NW and staying on the NW path throughout the transport process take up a relatively smaller proportion compared to the other two pathways and do not show any significant variation trends throughout the 2 decades. Trajectories turning to the W sector are most common and they are gaining in frequency in spring, autumn, and winter, with autumn showing the largest increasing slope ($0.79\,\% \, \mathrm{yr}^{-1}$). Trajectories staying in the NW and those bending to the W are more likely to keep their original air-mass properties and may therefore show higher ozone concentrations than the air masses turning to the E sector. Our previous work (Xu et al., 2016) shows that the largest ozone increase occurs in autumn, followed by spring, and the increasing trend in summer is not significant. This may be partly explained by the fact that the 168 h NW trajectory frequency increase is not as large in summer as in spring and autumn and more NW trajectories are turning to the E sector (low ozone) during summer than in the other seasons.

3.2 Impacts of stratospheric exchange versus regional anthropogenic emission trends

We next examine a suite of GFDL AM3 simulations designed to isolate the response of ozone to changes in meteorology, stratospheric exchange, and anthropogenic emission trends. Figure 4 shows year-to-year variation and long-term trends in observed and modelled ozone at WLG, as well as the modelled stratospheric contribution (O_3Strat) for the four seasons over the period of 1980–2014. GFDL AM3 captures some inter-annual variation in observed surface ozone anomaly, with the correlation coefficient ranging from 0.5 to 0.7 for spring, summer, and autumn. The correlations between the observed and modelled ozone anomaly are significant at the 90 % confidence level in all seasons except winter. The model fails to reproduce the small observed ozone variability in winter. The modelled ozone trends during 1994 to 2013 are $0.30 \pm 0.10\,\mathrm{ppbv}\,\mathrm{yr}^{-1}$ for spring, $0.25 \pm 0.10\,\mathrm{ppbv}\,\mathrm{yr}^{-1}$ for summer, $0.26 \pm 0.11\,\mathrm{ppbv}\,\mathrm{yr}^{-1}$ for autumn, and $0.13 \pm 0.16\,\mathrm{ppbv}\,\mathrm{yr}^{-1}$ for winter. Compared with the observed ozone trends, the modelled spring, summer, and winter trends are slightly overestimated, while the autumn trend is slightly underestimated, but the overall increasing trend is well reproduced by the model.
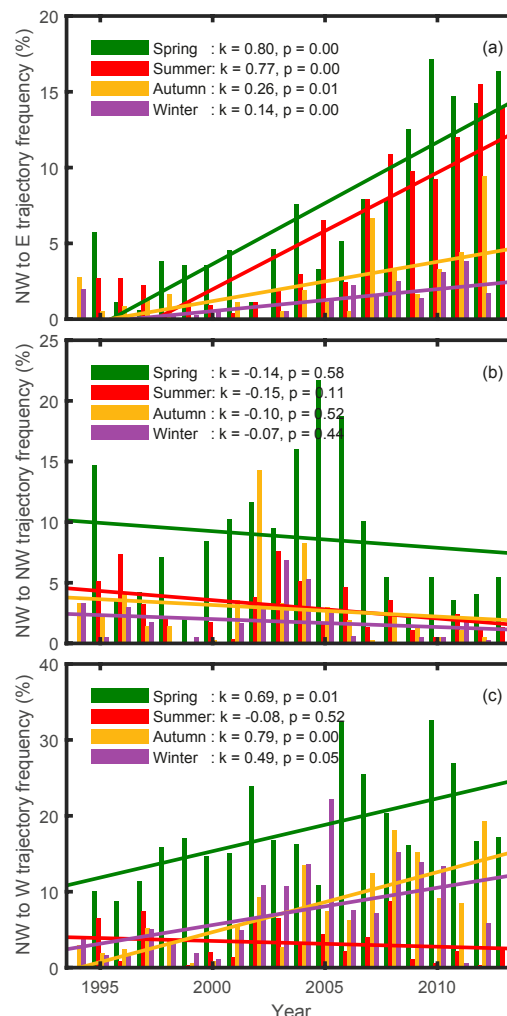

Figure 3. The occurrence frequency of trajectories whose average 168 h direction is NW and 24 h direction is E **(a)**, NW **(b)**, and W **(c)** in spring (green), summer (red), autumn (orange), and winter (purple). Bars stand for the occurrence frequencies while lines are their corresponding linear trends.

A stratospheric ozone tracer implemented in GFDL AM3 (O_3Strat; Sect. 2.5) enables us to quantify the stratospheric contribution to variability and trends in ozone measured at WLG. Prior analysis of daily ozonesondes, water vapour, and lidar measurements indicates that variability in AM3 O_3Strat represents the episodic, layered structure of ozone enhancements in the free troposphere consistent with the observed characteristics of deep stratospheric intrusions (Lin et al., 2012b, 2015a; Langford et al., 2015). Sampling AM3 O_3Strat at WLG indicates that the stratospheric influence can explain 23 % ($r = 0.48$) of the observed ozone inter-annual variability at WLG in spring (Fig. 4a) but contributes little to observed variability in other seasons ($r < 0.1$; Fig. 4b–d). AM3 O_3Strat shows an increasing trend
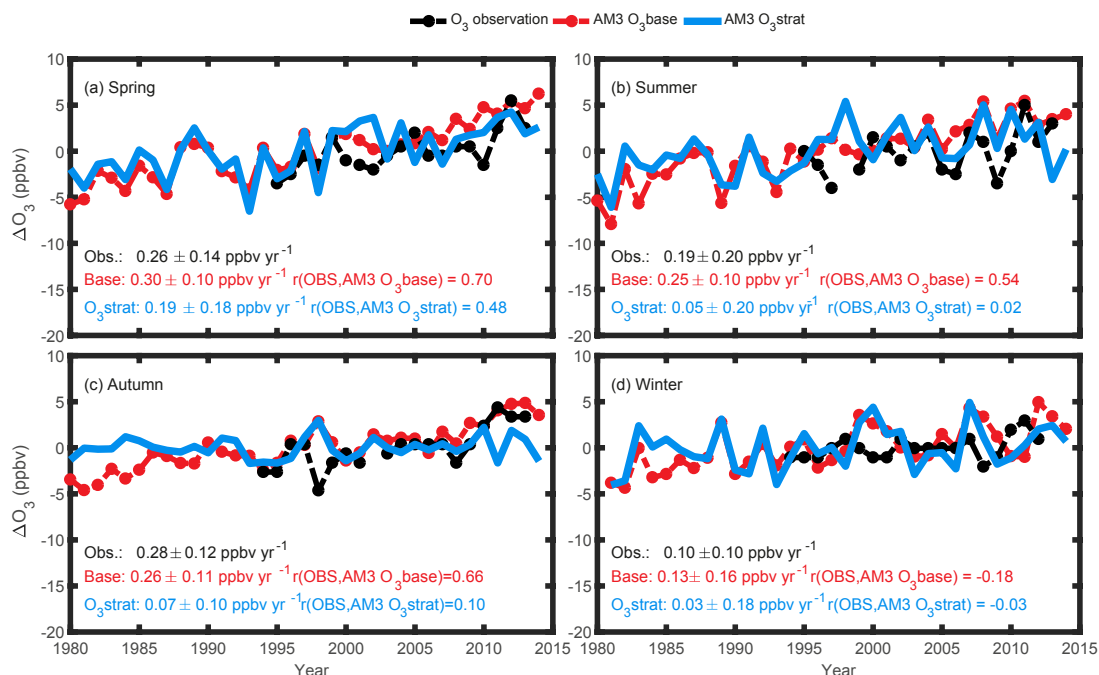
Figure 4. Comparison of seasonal median ozone anomalies at Mt Waliguan over the period of 1980–2014 from available observations (black), GFDL AM3 BASE simulations (red), and AM3 stratospheric ozone tracer (O_3Strat, blue) for **(a)** spring, **(b)** summer, **(c)** autumn, and **(d)** winter. The linear trends (with the 95 % confidence intervals) over the period of 1994–2013 and correlations between observations and models are shown.
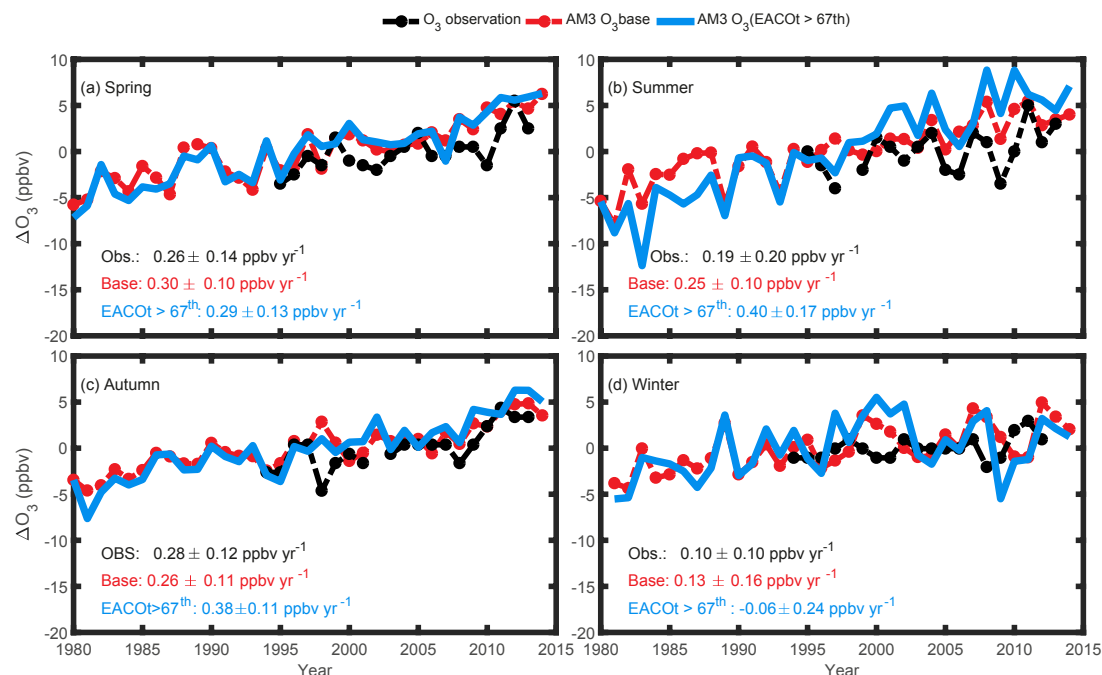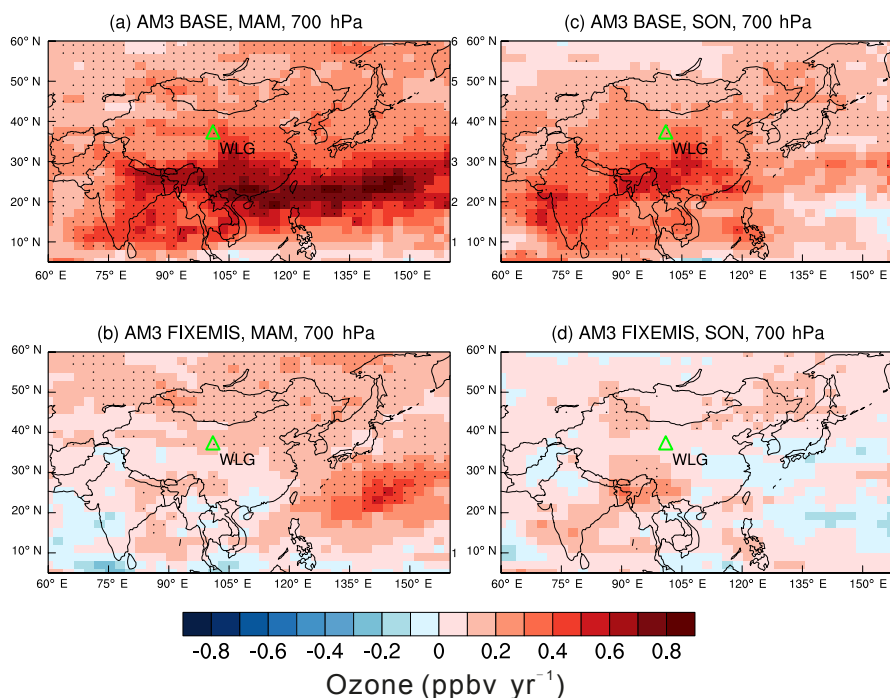

Figure 5. Comparison of seasonal median ozone anomalies at Mt Waliguan over the period of 1980–2014 from available observations (black), GFDL AM3 BASE simulations (red), and under conditions with strong transport from East Asia (EACOt > 67th, blue) for **(a)** spring, **(b)** summer, **(c)** autumn, and **(d)** winter. The linear trends (with the 95 % confidence intervals) over the period of 1994–2013 and correlations between observations and models are shown.

Figure 6. (a–b) The 1995–2014 trends of springtime average ozone sampled at 700 hPa as simulated by the GFDL AM3 model with time-varying (BASE) and constant anthropogenic emissions (FIXEMIS). **(c–d)** Same as **(a–b)** but for autumn. Triangles denote the location of WLG. Stippling indicates areas where the trend is statistically significant at the 95 % confidence level.

of 0.19 ± 0.18 ppbv yr^{-1} ($p < 0.05$) over the 1994–2013 period during spring, which can explain 59 % of the simulated ozone trend, indicating the importance of stratosphere-to-troposphere transport (STT) on rising springtime surface ozone measured at WLG over the past 2 decades (Fig. 4a). The largest stratospheric influences are found in the springs of 1999 and 2012 when O$_3$Strat shows an enhancement coinciding with the observed high ozone anomaly (Fig. 4a). We will further discuss the mechanisms driving these ozone enhancements in Sect. 4. During the other seasons, in contrast, O$_3$Strat reveals insignificant trends at the 95 % confidence level and shows weak correlations with the observed ozone (Fig. 4b–d). These results indicate that ozone from STT is the dominant contributor to the modelled increase in springtime ozone at WLG but it cannot explain the observed significant ozone increases in autumn.

To evaluate the effect of pollution transport from South East and East Asia, we filter ozone in the AM3 BASE simulation with the East Asian CO tracer (EACOt; see Sect. 2.5). Following the approach of Lin et al. (2015b, 2017) for western US sites, we use EACOt to identify days when WLG is strongly influenced by polluted airflow from South East Asia (including China) (i.e. EACOt greater than its 67th value during each season). Figure 5 shows the trends of ozone from observations, the BASE simulations, and the simulated ozone trends under conditions with strong transport from South East Asia (O$_{3,EA}$)

for the four seasons. During autumn, the simulated trend of ozone increases to 0.38 ± 0.11 ppbv yr^{-1} under the dominant influence from South East Asian air masses, compared to 0.26 ± 0.11 ppbv yr^{-1} from the BASE simulation and 0.28 ± 0.12 ppbv yr^{-1} from observations (Fig. 5c). Similar increases are found for summer when the model is filtered for the East Asian influence (Fig. 5b). In contrast, the simulated ozone trend at WLG during spring shows little change from the BASE simulation when filtered for the South East Asian influence (Fig. 5a), supporting our previous conclusion that the stratospheric influence is an important driver of springtime ozone trends measured at WLG (Fig. 4a). We do not expect a decrease in springtime ozone when filtering the model for the East Asian anthropogenic influence, i.e. air masses with lower stratospheric influence, owing to the offsetting effects of increasing East Asian emissions.

To separate the influences of changes in transport patterns and anthropogenic emission trends, we compare trends of seasonal mean ozone at 700 hPa simulated by GFDL AM3 with time-varying (BASE) and constant anthropogenic emissions (FIXEMIS) over 1995–2014 (Fig. 6). With both emissions and meteorology varying, AM3 BASE simulates increasing free tropospheric ozone trends of as large as 1 ppbv yr^{-1} throughout South East Asia and northern Asia for both spring and autumn (Fig. 6a and c). With emissions held constant in time, AM3 FIXEMIS shows very weak and insignificant ozone trends in South East Asia below 30° N

latitude (Fig. 6b and d). During spring, however, FIXEMIS simulates significant ozone increases of 0.2 ppbv yr^{-1} extending from Siberia to northeastern China and to the subtropical Pacific Ocean (Fig. 6b). This finding is consistent with our time series analysis that increasing ozone in the northwest flow from STT contributes to raising springtime ozone at WLG (Figs. 3a and 4a). The stratospheric influence can explain two-thirds of the total ozone increase at WLG in spring, with increases in Asian emissions contributing the other one-third. During autumn, AM3 shows strong ozone increases across the Asian continent in the BASE simulation but simulates few overall ozone trends (< 0.05 ppbv yr^{-1} around WLG) in FIXEMIS (Fig. 6c versus 6d), indicating that the observed autumnal ozone increase at WLG reflects the influence from increases in regional anthropogenic precursor emissions in South East Asia as opposed to changes in air-mass origin.

In summary, the AM3 modelling results clearly show that the spring and autumn increases in WLG surface ozone are governed by different processes. Observed increases in springtime ozone at WLG over the 1994–2013 period are linked to decadal variability in stratospheric ozone input in the northwest airflow, while the autumnal increase in ozone at WLG results from pollution transport from South East Asia, where NO$_x$ emissions have increased markedly over the last 2 decades. Notably, surface ozone increases during autumn in AM3 BASE are most pronounced over the subtropical South East Asian regions (south of $35°$ N; Fig. 7a), consistent with the observed surface ozone increase at Hong Kong in South China during autumn (Wang et al., 2009). The model shows somewhat decreasing surface ozone trends in the North China Plain during autumn (Fig. 7a), consistent with observations at Shangdianzi near Beijing and Lin'an near Shanghai (data not shown), indicating a NO$_x$-saturated ozone production. This north-to-south transition from NO$_x$-saturated to NO$_x$-sensitive O$_3$ production regimes during non-summer seasons has also been observed over the eastern US (Lin et al., 2017). Increasing ozone produced from regional anthropogenic emissions in South East Asia during autumn is lofted into the FT via deep convection and mid-latitude storms and is further transported in southern and southwesterly airflow towards WLG (Fig. 7b). This interpretation is consistent with one previous modelling study showing that WLG is more heavily influenced by pollution transported from South East Asia in autumn than in spring (Liu et al., 2002).

3.3 Impacts of background ozone transport versus local precursor emissions

We next examine the impacts of local photochemical production versus large-scale background ozone transport to WLG. The impact of direct ozone transport on ozone trends at WLG are studied by combining the 3-D TOST data from Liu et al. (2013) with the back trajectory analysis (Sect. 2.4). Differ-
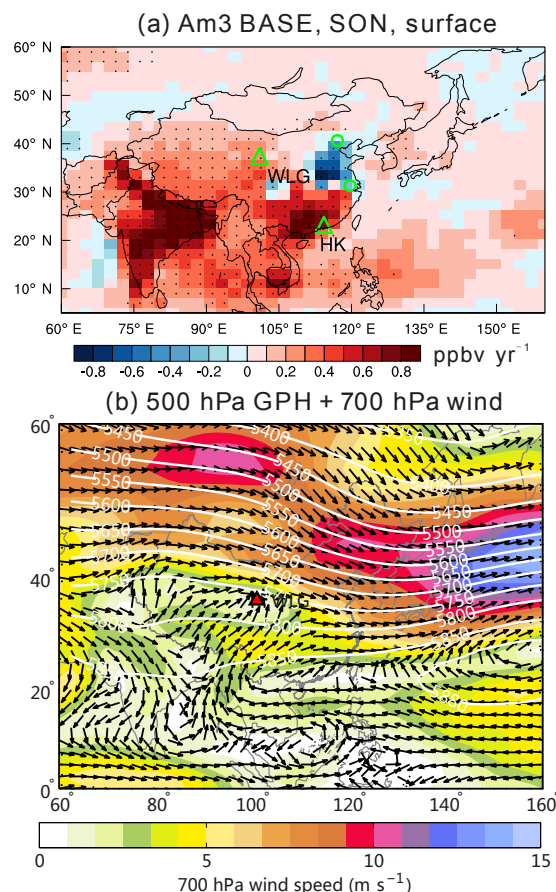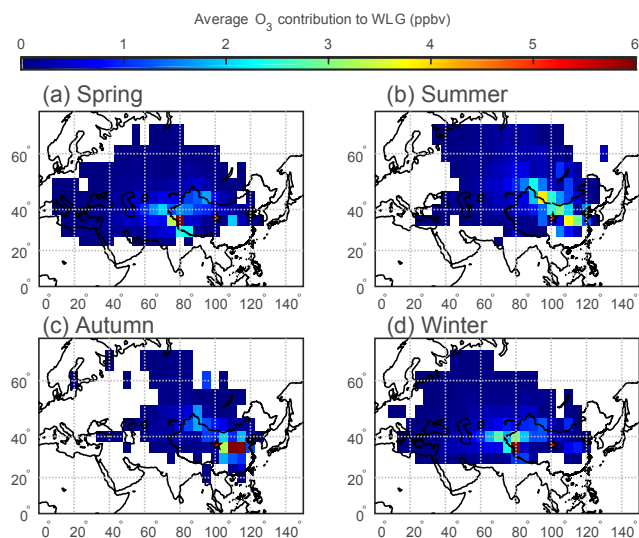

Figure 7. (a) The 1995–2014 trends of autumn average daily maximum 8 h average ozone sampled in the surface level from the GFDL AM3 model with time-varying anthropogenic emissions (BASE). Stippling indicates areas where the trend is statistically significant at the 95 % confidence level. Green symbols denote the locations of WLG, Hong Kong, Shangdianzi, and Lin'an. **(b)** Mean 700 hPa wind speed (colour shading), direction (black arrows), and 500 hPa geopotential height (contours) in autumn averaged over the 1994–2013 period.

ent from the GFDL AM3 FIXEMIS simulation discussed in Sect. 3.2, the TOST approach discussed in this section does not eliminate the impacts from increases in Asian anthropogenic emissions. The TOST data set is based on trajectory-mapped ozone soundings (Liu et al., 2013). The monthly averages of ozone in each grid should contain signals of background ozone and ozone produced within the grid from precursors emitted by anthropogenic and natural sources. Therefore, mean values in the TOST data set account for not only ozone changes due to transport but also ozone changes associated with varying global to regional anthropogenic and natural emissions.
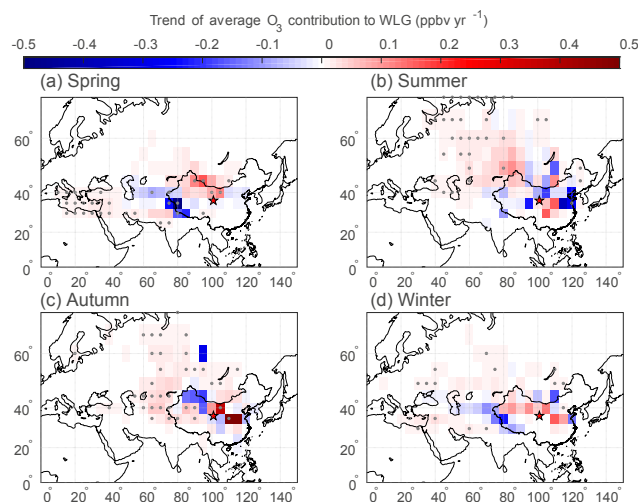
Table 2. Trend of total contribution of direct ozone transport to WLG ozone concentration (ppbv yr^{-1}); confidence intervals are given for $p < 0.1$.

Season	All year	Spring	Summer	Autumn	Winter
Slope	0.28 ± 0.30	0.27 ± 0.30	0.16 ± 1.11	0.56 ± 0.54	0.01 ± 0.32
P value	0.12	0.13	0.80	0.09	0.98

Figure 8. Average seasonal distributions of ozone contribution to WLG through direct transport of ozone during 1994–2013.

Figure 9. Average seasonal distributions of the trend of ozone contribution to WLG through direct transport of ozone during 1994–2013; grey dots stand for the grid cells with $p < 0.05$.

The seasonal average distribution of ozone contribution to WLG through direct tropospheric transport during 1994–2013 is shown in Fig. 8. It can be noted that the distribution varies with season. For winter and spring, the TOST analysis indicates major contributions from the western edge of the Tibetan Plateau and a small contribution from central China to the east of WLG (Fig. 8a). Large contributions from the northwestern to eastern sectors are found in summer, including contributions from Mongolia, Inner Mongolia, and central and eastern China, where high ozone levels can be observed during summertime. During autumn, WLG is strongly influenced by transport from central and eastern China and less influenced by the NW sector. This finding is consistent with the AM3 attribution results that increases in East Asian anthropogenic emissions contribute to raising autumnal ozone measured at WLG.

Figure 9 shows the trends of the ozone transport contribution in different seasons based on the TOST analysis. Spring shows a significantly increasing contribution from the north to northwest of WLG and a significantly decreasing contribution from the western sector, where the average contribution in spring is largest (see Fig. 8a). Statistically significant increases with small slopes were found in central Asia and eastern Europe during summer and winter (Fig. 9b, d).

Significant increasing trends in ozone contribution with relatively large slopes (> 0.5 ppbv yr^{-1}) can be seen in central and eastern China during autumn, while slower increases exist in the western, northwestern, and northern sectors.

Table 2 summarises the total contribution of direct ozone transport to WLG ozone concentration for each season for the annual mean. The rate of ozone change derived from the TOST data set for spring (0.27 ± 0.30 ppbv yr^{-1}) and summer (0.16 ± 1.11 ppbv yr^{-1}) agrees well with those derived from in situ observations at WLG (Xu et al., 2016); however, the trends derived from the TOST data sets are not statistically significant. This suggests that while important, the transport contribution is highly variable or that the uncertainty in this calculation method is large. The autumn trend from TOST (0.56 ± 0.54 ppbv yr^{-1}) is much larger than the observed trend (0.28 ± 0.11 ppbv yr^{-1}) and is relatively significant ($p < 0.1$), indicating that tropospheric ozone transport has elevated the level of autumn ozone at WLG. No trend was detected in winter, indicating that the ozone trend observed at WLG during winter cannot be attributed to tropospheric ozone transport.

One of the key issues in producing the TOST data set was the impact of ozone production along the trajectories, which might cause errors in the mapped ozone data. A careful as-
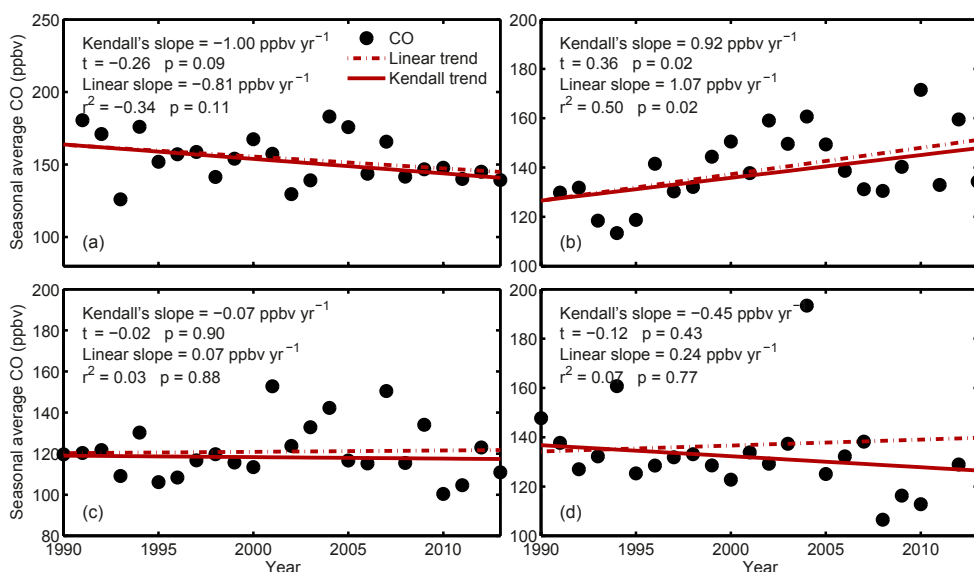
Figure 10. Mann–Kendall and linear trends of seasonal average CO observed during (**a**) spring, (**b**) summer, (**d**) autumn, and (**d**) winter from 1990 to 2013 at WLG.

sessment indicates that the errors are mostly small and insignificant (Liu et al., 2013). Our approach of using TOST data is similar to the forward mapping in Liu et al. (2013). Therefore, it is likely that the impact of ozone production along the trajectories during their residence time on our results is small, as in the case of Liu et al. (2013). As the bottom layer of the grid in which WLG resides is excluded in our calculations, direct impacts on our results from regional emissions in the grid containing WLG can be ruled out.

Local photochemical production can enhance O_3 at WLG if higher levels of O_3 precursors are transported to the site. Here we use monthly CO measurements at WLG to infer changes in ozone precursor emissions in cities nearby WLG. Figure 10 displays the trend of observed seasonal average surface CO at WLG during spring, summer, autumn, and winter. A statistically significant increase ($1.07\,\mathrm{ppbv\,yr^{-1}}$) is only found in summer. Since summer is the season when WLG is mostly influenced by easterly air masses, the rising CO level is most likely the result of growing anthropogenic emissions in the cities to the east of WLG. Note that trends in CO level reported here likely reflect changes in anthropogenic emissions in the cities near WLG rather than changes in anthropogenic emissions in eastern China.

To investigate the relative importance of the influence from the growing emissions east of WLG, the trajectories and the associated ozone concentrations were grouped into four groups (SW, NW, NE, and SE) according to the $t = -24\,\mathrm{h}$ trajectory directions. The trends and the according confidence intervals of the monthly average ozone concentrations associated with different air-mass origins were calculated using the seasonal Mann-Kendall trend analysis and listed in Table 3. It can be noted that the ozone associated with all

trajectory directions showed statistically significant upward trends during 1994 to 2013 at a confidence level of 95 %. The eastern sectors (NE and SE) display larger slopes than the western sectors (NW and SW). The largest ozone trend was associated with the SE direction, reaching 0.26 (0.19–0.34), 0.35 (0.26–0.44), and 0.28 (0.21–0.35) ppbv yr^{-1} for the all-day, daytime, and nighttime data subsets, respectively. The smallest ozone trend was associated with the NW direction, reaching 0.13 (0.08–0.19), 0.14 (0.07–0.19), and 0.11 (0.06–0.19) ppbv yr^{-1} for the all-day, daytime, and nighttime data subsets, respectively. This indicates that easterly trajectories, which are more likely to be influenced by anthropogenic emissions of ozone precursors, are associated with a larger ozone trend than westerly trajectories, suggesting that anthropogenic influence from the east also leads to the increase in ozone at WLG.

In all, the increase in ozone at WLG is influenced by both direct tropospheric ozone transport and rising precursor emissions in the eastern sector. The increase in direct transport of ozone to WLG only led to a significant rise in autumnal ozone, which supports the conclusions from the modelling study in Sect. 3.2.
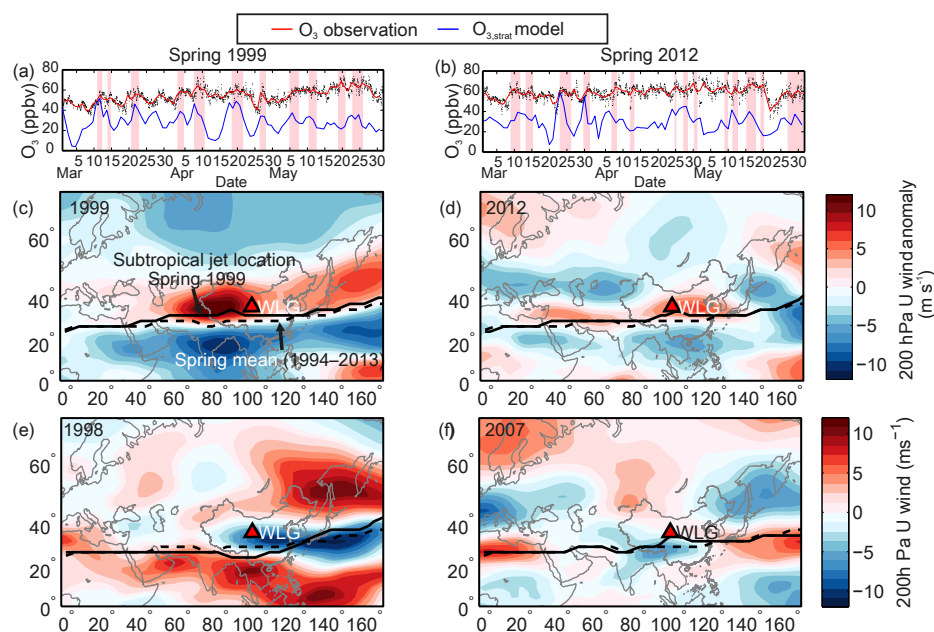
4 Atmospheric dynamics and ozone variability at WLG

4.1 Stratosphere-to-troposphere transport and jet characteristics

Due to the transient, localised nature of stratospheric intrusions, diagnosing the presence of stratospheric influence in near-surface ozone requires precise, high-frequency (a few

Table 3. The Kendall's variation slope (k, ppbv yr^{-1}) of ozone concentrations associated with different trajectory directions, the according confidence interval, and p values.

Variable	Time of day	Trajectory direction			
		SW	NW	NE	SE
k (ppbv yr^{-1})	all day	0.18	0.13	0.20	0.26
	day	0.17	0.14	0.28	0.35
	night	0.13	0.11	0.20	0.28
95 % confidence interval (ppbv yr^{-1})	all day	0.11–0.23	0.08–0.19	0.12–0.31	0.19–0.34
	day	0.13–0.23	0.07–0.19	0.15–0.41	0.26–0.44
	night	0.06–0.19	0.06–0.19	0.11–0.29	0.21–0.35
p	all day	< 0.01	< 0.01	< 0.01	< 0.01
	day	< 0.01	< 0.01	< 0.01	< 0.01
	night	0.01	< 0.01	< 0.01	< 0.01

Figure 11. Temporal variations in **(a)** hourly (black dots) and daily (red line) mean surface ozone observations and modelled O$_3$Strat (blue line) from March to May in 1999 and 2012; **(b)** 200 hPa zonal wind anomaly in the springs of 1999 and 2012 with the strong stratospheric influence; **(c)** same as **(a)** but for the springs of 1998 and 2007 with weak stratospheric influence.

minutes), and co-located measurements of ozone, CO, water vapour, and surface wind gust at remote sites (see Langford et al., 2015). These measurements are not available at WLG. Thus, we rely on a global model that has been previously shown to be able to represent deep stratospheric intrusions (Lin et al., 2012a, 2015a).

The highest ozone concentrations at WLG during spring were observed in 1999 and 2012, coinciding with the largest stratospheric influence simulated in the GFDL AM3 model (Fig. 4a). In contrast, the springs of 1998 and 2007 experienced lower observed ozone and simulated stratospheric influence. In this section we investigate the links of these

ozone anomalies to changes in the structure of the jet stream. The top panels of Fig. 11 show time series of observed daily surface ozone and modelled O$_3$Strat at WLG from March to May in 1999 and 2012, with the STT ozone transport events marked as the pink shades. During STT events, peaks are found in both observed surface ozone and modelled O$_3$Strat, accompanied mostly by enhancements in potential vorticity (PV) and ozone in the ERA-Interim data, as illustrated for 30 March 2012 (Fig. 12). A low-pressure system sat over northeastern China on 30 March 2012 (Fig. 12a). The WLG observatory was located ahead of a strong high-pressure ridge and behind the low-pressure trough. The
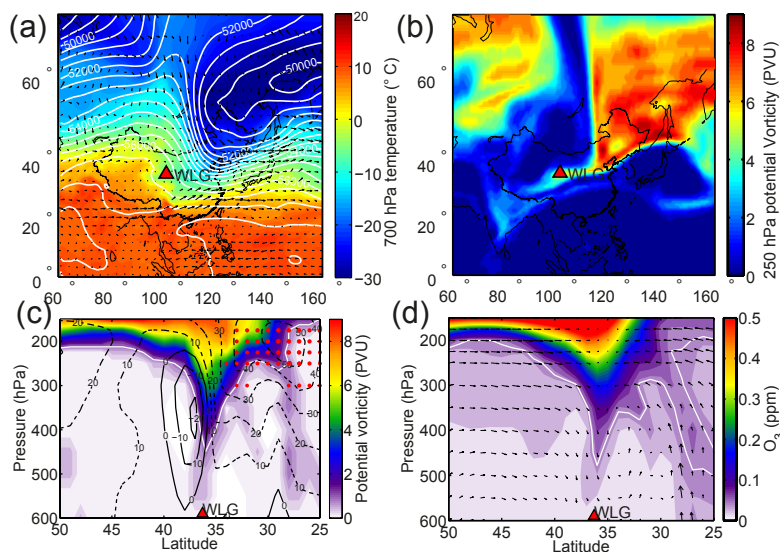
Figure 12. (a) Map of 500 hPa geopotential height (white contours), 700 hPa temperature (shading), and wind field (black arrows). **(b)** Map of 250 hPa potential vorticity; **(c)** the cross section of potential vorticity along the 101.0° E longitude line. The white line denotes the 1 PVU isoline, the black lines are U wind isolines (dashed lines for westerly winds and solid lines for easterly winds), and the red dots indicate the location of the subtropical jet stream (U wind $> 35\,\mathrm{m\,s^{-1}}$). **(d)** The cross section of ozone mixing ratios, V wind, and W wind vector along the 101.0° E longitude line from the ECMWF reanalysis during an STT transport event on 30 March 2012. The white line denotes the 50 ppbv ozone contour.

strong northerly airflow behind the low-pressure system and ahead of the ridge led to the transport of a high-PV air mass to the south, which is clearly visible on the 250 hPa PV field (Fig. 12b). A filament of high PV bends to the west and reaches up to 7 PVU over WLG. The mid-latitude jet stream (U wind $> 35\,\mathrm{m\,s^{-1}}$; red dots in Fig. 12c) extended up to 33° N, with a tropopause fold found to its north. Easterly airflows can be detected north of the tropopause fold, which together with the subtropical jet stream has forced the high-PV air mass to bend to the west at the latitude of WLG, directly influencing the STE process over WLG. The cross section of ozone from ECMWF shown in Fig. 12d displays a similar contour shape to the PV cross section and strong downward winds over WLG, indicating downward intrusions of stratospheric ozone into the troposphere.

Analysis of 200 hPa zonal wind anomalies from the NCEP reanalysis indicates strengthening of the mid-latitude jet stream across the Tibetan Plateau during the springs of 1999 and 2012, with the centre of the jet stream shifted to the north towards WLG compared to the 1994–2013 mean state (Fig. 11b). These circulation anomalies facilitate the formation of tropopause folding and transport of stratospheric ozone into the FT above WLG, consistent with frequent STT events as identified by GFDL AM3 O_3Strat (Fig. 11a). For comparison, the strength of the jet stream across the Tibetan Plateau was weakened during the springs of 1998 and 2007, leading to weaker stratospheric influence at WLG. In particular, the location of the subtropical jet was shifted to the
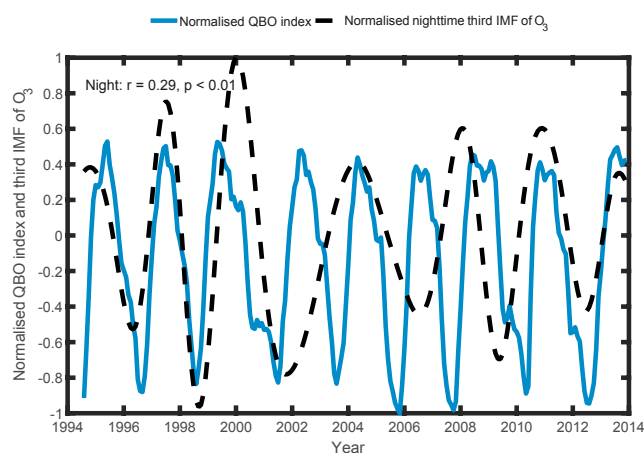

Figure 13. Comparison between the normalised nighttime (dashed black line) third IMF and the normalised 30 hPa QBO index (solid blue line) during 1994–2013.

south far away from WLG in spring 1998 following a strong El Niño winter. These interpretations are consistent with the findings of Lin et al. (2015a), who showed frequent stratospheric intrusions and high-surface-ozone events during the springs of 1999 and 2012 when the polar jet stream was unusually contorted over the western US. Stratospheric intrusions over the subtropics are found most frequently along the subtropical jet stream, where the tropopause break is located (e.g. Homeyer, 2012; Sprenger and Wernli, 2003).
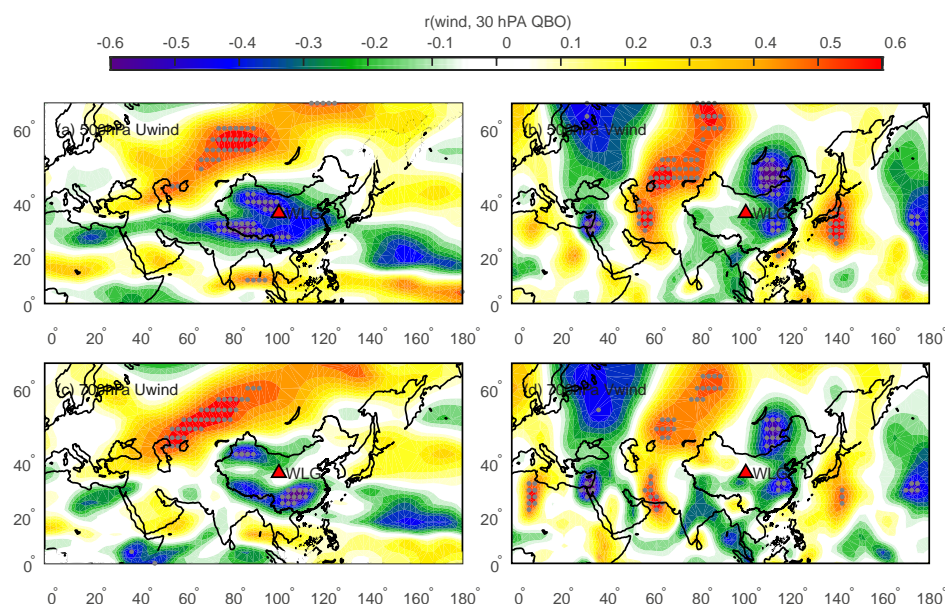
Figure 14. Correlation coefficients between the QBO index and zonal **(a, c)** and meridional **(b, d)** wind at 500 and 700 hPa with grey dots indicating those that are significant ($p < 0.05$). The red triangles indicate the position of WLG.

Tropopause folds are typically located to the north of the subtropical jet stream; hence the location of the jet stream directly influences the location of the STE event. If the jet were located more to the south, the stratospheric ozone input might not reach WLG. For the springs of 1999 and 2012, the average subtropical jet locations (latitude) at the longitude of WLG for STE cases are, respectively, 2.5 and 3.4° more north than those for non-STE cases. This supports the view that the shift of the jet to the north pushes the location of the tropopause folding to the north, which then leads to STE processes over the WLG region.

4.2 Modes of atmospheric circulation

The time series of surface ozone at WLG was decomposed into five intrinsic mode functions (IMFs) with different periodicities using the HHT analysis in combination with the empirical mode decomposition (EMD) (Xu et al., 2016). The first IMF shows high frequency, representing variations associated with synoptic systems. The second IMF, with a periodicity of 1 year, represents seasonal variation and made the largest contribution to the variability in ozone. The other IMFs played minor roles in the variations in ozone. However, these IMFs are interesting because they are related to the 2–4-, 7-, and 11-year periodicities found in the ozone data and contribute to the inter-annual variability in ozone at WLG. There are many oscillations within the atmospheric circulation with different periodicities, e.g. QBO with a quasi-2-year periodicity and ENSO with a 2- to 7-year periodicity (Xu et al., 2016). Here, we explore potential links of some atmospheric circulation oscillations to the variations in surface ozone at WLG (Xu et al., 2016). Since nighttime ozone

concentrations at WLG are more representative of the free-tropospheric air condition, IMFs of the nighttime ozone data are applied in the following analysis.

Previous studies concluded that column ozone over the Tibetan Plateau bears a QBO signal with the same phase as the tropical stratospheric wind QBO, which is caused by the increase and decrease in tropopause height over the Tibetan Plateau region, as the tropical stratospheric winds shift from easterly to westerly (Ji et al., 2001). The third IMF of the nighttime surface ozone data reveals a periodicity closest to that of the QBO index. The comparison between the QBO index and the third IMF is displayed in Fig. 13. It can be discerned that the normalised third IMF and the QBO index show a positive correlation during nighttime ($r = 0.29$, $p < 0.01$). The peaks and valleys coincide well with each other during 1994–2002 and 2011–2013. During 2003–2010, the QBO index displays four peaks, while the third IMF only shows two peaks. This suggests that surface ozone at WLG was indirectly linked to the QBO; however, the EMD analysis was not fully able to extract the QBO signal during 2003–2010 probably due to the interference of other signals or the abnormally long QBO period from 1998 to 2001. This link of surface ozone to the QBO cannot be explained by the finding of Ji et al. (2001) because surface ozone is independent of TCO and the GFDL AM3 O_3 Strat is not correlated with the QBO index.
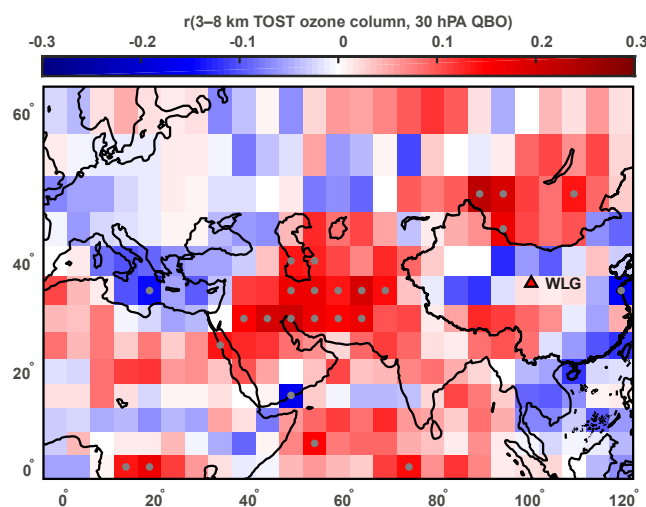
Although the QBO is an atmospheric oscillation in the stratosphere, its dynamical and chemical effects are not limited to the stratosphere but can propagate downward to the Earth's surface and upward to the mesosphere (Baldwin et al., 2001). Some mechanisms have been proposed to show

Table 4. Correlation between the surface ozone (1994–2013), NCEP reanalysis precipitation (1990–2015), and EASMI (1990–2015).

r (p value)	June	July	August
Precipitation & EASMI	−0.12 (0.15)	−0.47 (0.02)	0.21 (0.12)
O_3 & EASMI	−0.08 (0.76)	−0.59 (0.01)	−0.32 (0.20)
O_3 & precipitation	0.30 (0.10)	−0.01 (0.20)	−0.51 (0.03)

how the QBO can change the large-scale circulations and exert impacts on tropospheric winds, temperature, etc. (e.g. Collimore et al., 2003; Kwan and Samah, 2003). To see the possibility of a QBO influence on surface ozone at WLG, correlations between the QBO index and zonal as well as meridional wind were calculated for different pressure levels. Figure 14 shows the correlation coefficients for the 500 and 700 hPa levels. As can be seen in Fig. 14, there is a large zone of positive correlation between the annual QBO index and zonal winds at both levels, extending from western Asia to central Asia to the middle of Russia. There is also a large zone of positive correlation between the annual QBO index and meridional winds at both levels, extending from the north of the Indian Ocean to central Asia to Russia. The results suggest that when the QBO is in its positive phase, westerly and southerly winds over large areas west, northwest, and north of China are increased. Similar zones of positive correlations also exist between the annual QBO index and air temperatures at different pressure levels, with a warming of 0.01–0.04° per unit increase in the QBO index (Fig. S2). These periodic changes in air circulations and temperature might have influenced the transport of ozone and its precursors and the photochemical conditions. In fact, we can see significant positive correlations of the QBO index with the 3–8 km TOST ozone columns over some areas west and north of China (Fig. 15). As the FT air over these areas can influence surface ozone at WLG through long-range transport (see Fig. 1), we can expect a small signal in ozone at WLG that is related to the periodic changes in tropospheric ozone over areas west and north of China, caused indirectly by the QBO. The third IMF reported in Xu et al. (2016) may be such a signal. There are other ways that the QBO influences the ozone distribution. For example, Hudson (2012) reported that the QBO can cause a few degrees of poleward movement of the subtropical jet streams and a shift of the subtropical front towards the pole. At present, it is not clear whether or not this mechanism influenced our ozone measurement. To better understand the QBO influence on surface ozone at WLG, a comprehensive modelling study is necessary, which is out of the scope of this paper.

The EASM, ENSO, and other circulation-related factors might influence surface ozone at WLG through the change of the precipitation or via STE processes. However, these influencing factors are often coupled with each other and a direct relationship between surface ozone observations and these factors might be hard to determine.

Figure 15. Correlation coefficients between the QBO index and the 3–8 km TOST ozone columns. Correlations for the grids with grey dots indicating those that are significant ($p < 0.05$).

The correlation coefficients between surface ozone concentrations, precipitation, and the EASM index (EASMI) for June, July, and August is listed in Table 4. Only during July could a significant negative correlation ($r = -0.59$, significant at a 99 % confidence level) be detected between the ozone concentration and the EASMI, which coincides with the significant correlation between the precipitation rate and the EASMI ($r = -0.47$, significant at a 95 % confidence level). However, no significant relationship was found between ozone and precipitation, indicating that the precipitation might not be the only or the most dominant process through which the EASM influences ozone.

To investigate the possible impact of the EASM on the STT processes at WLG, the average location of the subtropical jet stream for the top and bottom 15th percentile EASMI cases and the correlation coefficients between the 200hPa zonal wind and the EASMI in June, July, and August from 1990 to 2015 were calculated and are displayed in Fig. 16a, c, e. The jet stream location (dashed and solid black lines in Fig. 16a) near WLG does not change in June for strong (EASMI > 85th) and weak (EASMI < 15th) EASM years; however, a significant positive correlation band between the zonal wind and the EASMI is found over WLG along the subtropical jet, indicating that during strong EASM years, the subtropical jet stream strengthens as well. In July and
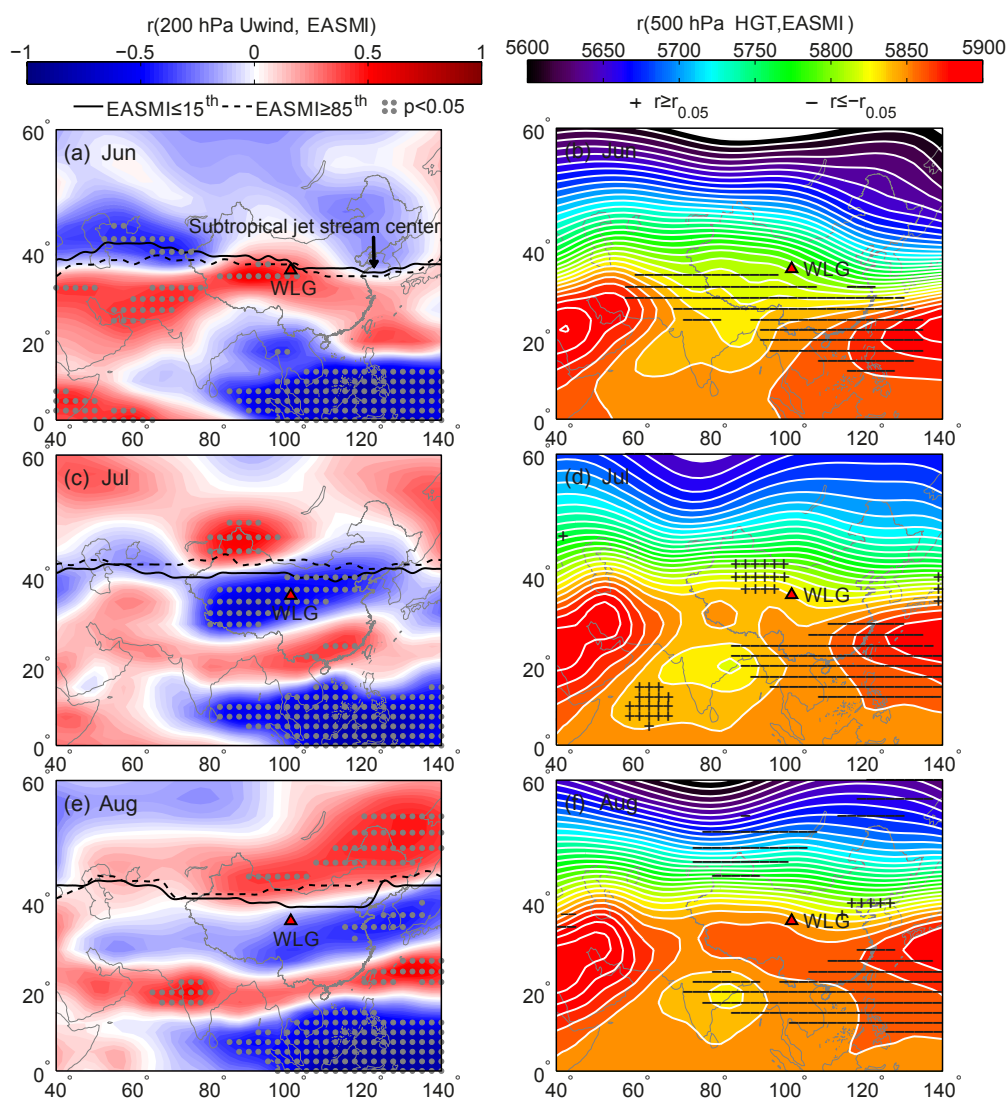
Figure 16. (a, c, e) The correlation coefficient between the 200 hPa zonal wind and the EASMI and the average location of the subtropical jet stream centre for the EASMI ≤ 15th percentile and EASMI ≥ 85th percentile cases and **(b, d, f)** the average 500 hPa geopotential height and the location of significant positive(+) and negative(−) correlation ($p < 0.05$) between 500 hPa geopotential height and the EASMI in **(a, b)** June, **(c, d)** July, and **(e, f)** August during 1990 to 2015.

August, the subtropical jet stream shifts north away from WLG during strong EASM years and shifts to the south towards WLG during weak ones. In July, the jet stream during weak EASM years is associated with a significant negative correlation between zonal wind speed and EASMI, indicating that the jet gains strength during weak EASM years. The shift in subtropical jet stream location leads to changes in STT, which is confirmed by the simulation results of the stratospheric contribution (Table 5). The modelled monthly O_3Strat data were associated with the EASMI to filter out O_3Strat for weak and strong monsoon years. Results reveal that O_3Strat concentrations during weak monsoon years are 10, 19, and 27 % higher than those during strong monsoon years in June, July, and August, respectively.

The EASM can also change the atmospheric circulation and thus change transport processes over WLG. The average 500 hPa geopotential height distribution is shown in Fig. 16b, d, f and the locations where the geopotential height is significantly correlated to the EASMI are marked by + and − signs according to the sign of the correlation coefficients. It can be seen that WLG is located behind a ridge, which is why WLG is often governed by northwesterly air flows. The centre of the western Pacific subtropical high-pressure belt shifts northwards during June to August. At the same time a strong low-pressure system forms over India and reaches its strongest state in July. The location of the convergence belt between the Indian low and the subtropical high seems to favour transport from eastern China during July. Strong neg-

Table 5. The changes in stratospheric ozone input and in ozone concentration associated with East Asian, European, and North American transport (%) introduced by the East Asian summer monsoon. The average ozone values associated with the EACOt $\geq$ 67th, EUCOt $\geq$ 67th, and NACOt $\geq$ 67th are used to represent the ozone transported from East Asia ($O_{3, \text{ea}}$), Europe ($O_{3, \text{eu}}$), and North America ($O_{3, \text{na}}$). The East Asian summer monsoon index (EASMI) is used to filter out those $O_{3, \text{ea}}$, $O_{3, \text{eu}}$, and $O_{3, \text{na}}$ values associated with the lower and upper 15th percentiles of EASMI. The relative change induced by the East Asian Monsoon is then calculated with the equation ($O_{3, \text{EASMI}} < = 15\text{th}$-$O_{3, \text{EASMI}} > = 85\text{th}$) / $\bar{O}_3$.

Month	$(O_{3, \text{EASMI}<=15\text{th}}$-$O_{3, \text{EASMI}>=85\text{th}})$ / $\bar{O}_3$ (%)					
	O_3Strat	$O_{3, \text{ea}}$	$O_{3, \text{eu}}$	$O_{3, \text{na}}$	Mean	$O_{3, \text{WLG}}$
Jun	10.4	−6.2	1.3	−3.8	0.4	−0.5
Jul	18.9	6.2	0.1	4.3	7.4	8.7
Aug	26.6	−0.4	−3.2	−3.2	4.9	4.5

Figure 17. Comparison between the fifth IMF and the 1-year running average SSN during 1994–2013.

ative correlation exists between the EASMI and the 500 hPa geopotential height to the south of WLG during June to August, while in July the negative correlation exists mostly to the east of the Indian low. The negative correlation in July suggests that the subtropical high is enhanced during July in weak monsoon years, without weakening the Indian low. This is probably the cause of an increased ozone concentration (6 %) associated with high EACOt during weak monsoon cases in comparison to strong monsoon cases during July (Table 5). Additionally, increased ozone concentrations are also observed in those associated with high NACOt (4 %) during July. June and August both display decreased ozone concentrations associated with the high EACOt and NACOt during weak monsoon years.

In summary, weak monsoon years favour STT ozone transport, especially during July and August, and the circulation pattern during weak monsoon years favours the horizontal transport of ozone to WLG during July, which results in a strong negative correlation between the EASMI and the ozone concentrations in July. These results are in contrast with the modelling study by Yang et al. (2014), which suggested that summer ozone concentrations over the Tibetan Plateau were positively correlated to the EASMI.

4.3 The impact of solar activities

It is well known that changes in incoming solar ultraviolet radiation can cause solar cycle signals of ozone in the stratosphere (Maycock et al., 2016). A solar cycle signal was also found in the tropospheric ozone column data over the Tibetan Plateau (Huang et al., 2009), with an increase of 4 % in tropospheric ozone from the solar minimum to solar maximum. Here, we investigate the impact of solar activities on surface ozone trends at WLG by comparing the normalised 1-year running average SSN with the normalised daytime and nighttime fifth IMFs of monthly average ozone that were obtained
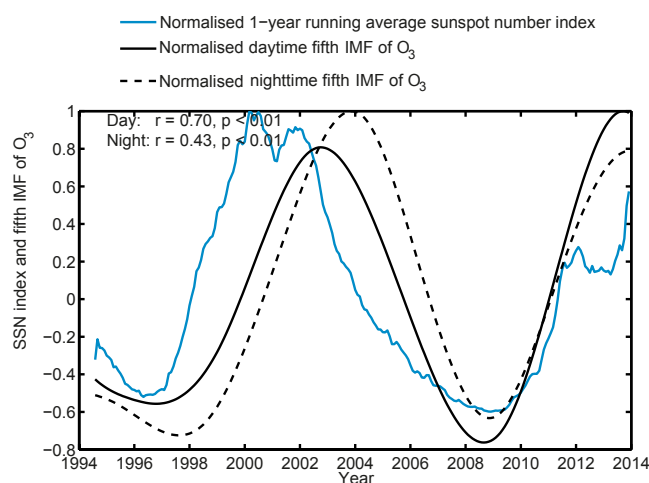
in our previous study (Xu et al., 2016). Results are displayed in Fig. 17, which shows that both the daytime and nighttime fifth IMFs are positively correlated to the SSN, with daytime ($r = 0.70$, $p < 0.01$) showing a better correlation than nighttime ($r = 0.43$, $p < 0.01$). During the 1994–2013 period, there were two valleys of the SSN in 1996 and 2008 and two broad peaks during 2000–2002 and 2012–2014. The occurrence time of the two valleys in the daytime fifth IMF agrees well with that of the SSN, while the first peak shows a delay of 1–2 years. The nighttime fifth IMF displays both a delayed valley in 1997 and a peak in 2004.

The positive correlation between the fifth IMF and the SSN explains the 11-year periodicity found in the ozone data. Solar activity led to surface ozone variations within the range of ± 0.5 ppbv over the period of 1994 to 2013 (see Fig. 6 in Xu et al., 2016). Both our results and those of Huang et al. (2009) indicate a positive impact of solar maximum on the ozone level. However, Chandra et al. (1999) obtained a 12.6 % reduction in tropospheric column ozone over the tropics from the solar minimum to solar maximum. They attributed this reduction to tropospheric ozone photochemistry under the condition of low NO_x and high relative humidity, modulated by changing UV radiation related to the solar cycle. The opposite effect would be expected in the high-NO_x regime over the Tibetan Plateau. However, details of the mechanism of the solar cycle response of tropospheric and surface ozone over the Tibetan Plateau remain to be investigated.

5 Multivariate regression of surface ozone at Waliguan

The analysis above suggests that surface ozone at WLG can be influenced by various factors. Some of these factors mainly disturbed the seasonal variation in ozone and contributed to the inter-annual differences, others also con-

Table 6. Multivariate regression coefficients (Eqs. 6–7) of the surface ozone at WLG.

Factor	Regression coefficients						
	t_0						
t	1.003						
	a_0	$a_{1,1}$	$a_{2,1}$	$a_{1,2}$	$a_{2,2}$	$a_{1,3}$	$a_{2,3}$
BKG	0.190	-0.250	0.229	0.028	-0.007	-0.005	-0.012
	$b_{i,0}$	$b_{i,1}$	$b_{i,2}$				
O_3Strat	0.336	-0.135	-0.109				
$O_{3,\,trop}$	0.100	0.042	-0.112				
SSN	0.057	-0.031	-0.055				
NW_{freq}	0.111	-0.048	-0.100				
QBO	0.021	-0.006	-0.018				

tributed to the observed long-term trends. To quantify the contributions of different factors to surface ozone at WLG, a multivariate regression was performed, with normalised monthly ozone concentration being a dependent variable and time and the potential influencing factors being independent variables. All candidate independent variables, e.g. the QBO index, the NAO index, the SSN, the modelled O_3Strat, the NW trajectory frequency (f(NW)), the SE trajectory frequency (f(SE)), and the calculated direct transport contribution of tropospheric ozone ($O_{3,\,trop}$), were converted to normalised monthly values. The regression equation takes the form described in Sect. 2.6.

The regression was conducted stepwise to avoid overfitting. The coefficient of determination (R^2) and residual sum of squares (RSS) were calculated after each step of the regression. Correlation coefficients were calculated between the residual and all remaining variables. The variable that correlates best with the residual was chosen as the next independent variable to be included in the model. The regression stopped when the changes in R^2 and RSS were less than 1 %. The first step of the regression was to fit the third-order harmonic function (Eq. 6) to the normalised ozone data. Five factors (i.e. O_3Strat, $O_{3,\,trop}$, SSN, f(NW), and QBO index) were successively included in the regression and became independent variables. Changes of R^2 and RSS after each step are shown in the supplement (Fig. S3). The regression coefficients are listed in Table 6. An empirical model for normalised monthly ozone at WLG is obtained by integrating the regression coefficients in Table 6 into Eqs. (5)–(7). This empirical model is used for the calculation of normalised monthly ozone at the site.

Figure 18 shows a comparison between the calculated and observed ozone, together with the calculated contributions of the influencing factors to the normalised monthly ozone at the site. It can be seen that the calculated normalised ozone reproduces the observed one well ($R^2 = 0.92$). The differences (residual) between the observed and calculated normalised ozone are within ± 0.25 and mostly within ± 0.10. An ozone trend of 0.25 ppbv yr^{-1} is obtained from the ob-

servational data, while the calculated ozone data give a trend of only 0.08 ppbv yr^{-1}. The discrepancy can partly be explained by the trend in the residual (0.11 ppbv yr^{-1}). The rest should be due to the uncertainties associated with the empirical model as well as the independents.

The regression found an annual variation in the normalised ozone with an amplitude of about 0.67 and no trend. The modelled O_3Strat, $O_{3,\,trop}$, SSN, f(NW), and QBO contribute up to 0.32, 0.17, 0.11, 0.12, and 0.04, respectively, to the calculated normalised ozone. These results indicate that the level of surface ozone at WLG has a basic component (the background signal), which makes the major contribution to the seasonal variation in ozone but has no long-term trend. The background signal is enhanced by varying contributions from STT, tropospheric ozone transport, and SSN, influenced by changes in the NW trajectory frequencies and very little by QBO.

6 Conclusions

Through an observational and modelling analysis, we have discussed the key drivers of various periodicities and long-term trends of ozone measured at WLG for the four seasons over the past 2 decades, previously reported in the companion paper (Xu et al., 2016). The impact of air-mass origin is investigated using backward trajectory analysis combined with PSCF analysis; the influence of STE and increasing anthropogenic emissions in Asia is evaluated using chemistry–climate model hindcasts driven by reanalysis winds (GFDL AM3; Lin et al., 2017). The impact of direct tropospheric ozone transport on ozone at WLG is examined using 3-D tropospheric ozone climatology data (a subset of TOST) combined with the trajectory analysis results.

Our results show that different processes have contributed to the observed increasing ozone trends at WLG during spring versus autumn. Analysis of a stratospheric ozone tracer in GFDL AM3 indicates that STT can explain ~ 60 % of the simulated springtime ozone increase over 1994–2013
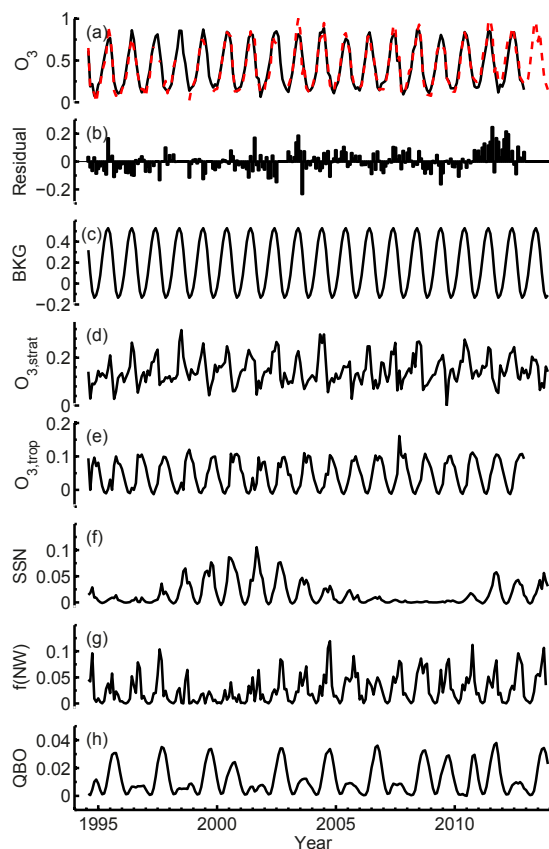
Figure 18. Temporal variation in the **(a)** normalised observed and fitted ozone concentration, **(b)** the residual of the regression, the contribution of **(c)** a background factor and five influencing factors to the ozone regression: **(d)** the modelled O$_3$Strat, **(e)** the contribution of tropospheric ozone transport O$_{3, \text{trop}}$, **(f)** the sunspot number, **(g)** the frequency of northwesterly trajectories, and **(h)** the QBO index.

at WLG (Fig. 4a). This interpretation is consistent with an increase in the NW air-mass frequency over this period inferred from the trajectory analysis (Fig. 3). STT contributes to the observed high ozone anomalies at WLG during the springs of 1999 and 2012 (Figs. 11 and 12), linked to the unusual structure of the jet stream as occurs over the western US during the same years (Lin et al., 2015a). During autumn, observations at WLG are more heavily influenced by polluted air masses originating from South East Asia than in the other seasons (Figs. 1 and 7). The GFDL AM3 model captures the observed ozone increase at WLG during autumn (0.26 ± 0.11 ppbv yr^{-1}) and simulates a greater ozone increase of 0.38 ± 0.11 ppbv yr^{-1} under conditions with strong transport from South East Asia (Fig. 5c), indicating that rising anthropogenic emissions of ozone precursors in South East Asia play a key role in raising ozone observed at WLG during autumn (Fig. 6). During summer, WLG is mostly influenced by easterly air masses from the cities to the east of WLG but these trajectories do not extend to the polluted

regions of eastern China and have decreased significantly over the last 2 decades (Fig. 2), which likely explains why summertime ozone measured at WLG shows no significant trend despite ozone increases in eastern China. The direct transport of tropospheric ozone to WLG calculated from the TOST data and trajectory residence time reveals significant increases during autumn mostly coming from the eastern sector (Table 2 and Figs. 8 and 9).

The periodicities detected in the HHT analysis of ozone data previously reported by Xu et al. (2016) are linked to various climate indices including EASMI, QBO, and sunspot cycle. The 2–3-year periodicity is linked to the QBO and the 3–7-year periodicity could be partly explained by the EASMI, while the 11-year periodicity is well connected to the sunspot cycle. An empirical model is obtained for normalised monthly level of surface ozone at WLG using the multivariate regression technique and is used to explain the observed ozone trends. Based on these relationships, an empirical model has been established for normalised monthly ozone through multivariate regression. The regression model reproduces the observation well and can capture about one-third of the observed ozone trend.

The results obtained in this work clearly show the complexity of surface ozone in terms of influencing factors. Comprehensive investigations are recommended to understand variations in surface ozone, in particular the long-term trends, at any site. Our work in this paper and the companion paper shows an example of de-convoluting the ozone variations and interpreting those using related dynamical and chemical factors of different scales, which can hopefully inspire similar studies.

References

Ara Begum, B., Kim, E., Jeong, C.-H., Lee, D.-W., and Hopke, P. K.: Evaluation of the potential source contribution function using the 2002 Quebec forest fire episode, Atmos. Environ., 39, 3719–3724, https://doi.org/10.1016/j.atmosenv.2005.03.008, 2005.

Baldwin, M. P., Gray, L. J., Dunkerton, T. J., Hamilton, K., Haynes, P. H., Randel, W. J., Holton, J. R., Alexander, M. J., Hirota, I., and Horinouchi, T.: The quasi-biennial oscillation, Rev. Geophys., 39, 179–229, https://doi.org/10.1029/1999RG000073, 2001.

Bonasoni, P., Evangelisti, F., Bonafe, U., Ravegnani, F., Calzolari, F., Stohl, A., Tositti, L., Tubertini, O., and Colombo, T.: Stratospheric ozone intrusion episodes recorded at Mt. Cimone during the VOTALP project: case studies, Atmos. Environ., 34, 1355–1365, https://doi.org/10.1016/S1352-2310(99)00280-0, 2000.

Chandra, S., Ziemke, J. R., and Stewart, R. W.: An 11-year solar cycle in tropospheric ozone from TOMS measurements, Geophys. Res. Lett., 26, 185–188, https://doi.org/10.1029/1998GL900272, 1999.

Collimore, C. C., Martin, D. W., Hitchman, M. H., Huesmann, A., and Waliser, D. E.: On The Relationship between the QBO and Tropical Deep Convection, J. Climate, 16, 2552–2568, https://doi.org/10.1175/1520-0442(2003)016<2552:otrbtq>2.0.co;2, 2003.

Creilson, J. K., Fishman, J., and Wozniak, A. E.: Intercontinental transport of tropospheric ozone: a study of its seasonal variability across the North Atlantic utilizing tropospheric ozone residuals and its relationship to the North Atlantic Oscillation, Atmos. Chem. Phys., 3, 2053–2066, https://doi.org/10.5194/acp-3-2053-2003, 2003.

Derong, Z., Aijun, D., Huiting, M., Congbin, F., Tao, W., Chan, L. Y., Ke, D., Yang, Z., Jane, L., An, L., and Nan, H.: Impacts of the East Asian monsoon on lower tropospheric ozone over coastal South China, Environ. Res. Lett., 8, 044011, https://doi.org/10.1088/1748-9326/8/4/044011, 2013.

Ding, A. and Wang, T.: Influence of stratosphere-to-troposphere exchange on the seasonal cycle of surface ozone at Mount Waliguan in western China, Geophys. Res. Lett., 33, L03803, https://doi.org/10.1029/2005GL024760, 2006.

Ding, A. J., Wang, T., Thouret, V., Cammas, J.-P., and Nédélec, P.: Tropospheric ozone climatology over Beijing: analysis of aircraft data from the MOZAIC program, Atmos. Chem. Phys., 8, 1–13, https://doi.org/10.5194/acp-8-1-2008, 2008.

Draxler, R. R.: HYSPLIT4 user's guide, NOAA Tech. Memo, ERL ARL-230, NOAA Air Resources Laboratory, Silver Spring, MD, 1999.

Draxler, R. R. and Hess, G. D.: Description of the HYSPLIT_4 modeling system, NOAA Tech. Memo, ERL ARL-224, NOAA Air Resources Laboratory, Silver Spring, MD, 24 pp., 1997.

Draxler, R. R. and Hess, G. D.: An overview of the HYSPLIT_4 modelling system for trajectories, dispersion and deposition, Aust. Meteorol. Mag., 47, 295–308, 1998.

Homeyer, C. R.: Chemical and Dynamical Characteristics of Stratosphere-Troposphere Exchange, Atmospheric Sciences, Texas A&M University, 2012.

Huang, F.-X., Liu, N.-Q., and Zhao, M.-X.: Solar Cycle Signal of Tropospheric Ozone over the Tibetan Plateau, Chinese J. Geophys., 52, 913–921, https://doi.org/10.1002/cjg2.1416, 2009.

Hudson, R. D.: Measurements of the movement of the jet streams at mid-latitudes, in the Northern and Southern Hemispheres, 1979 to 2010, Atmos. Chem. Phys., 12, 7797–7808, https://doi.org/10.5194/acp-12-7797-2012, 2012.

Itahashi, S., Uno, I., Irie, H., Kurokawa, J.-I., and Ohara, T.: Regional modeling of tropospheric NO_2 vertical column density over East Asia during the period 2000–2010: comparison with multisatellite observations, Atmos. Chem. Phys., 14, 3623–3635, https://doi.org/10.5194/acp-14-3623-2014, 2014.

Ji, C. P., Zou, H., and Zhou, L. B.: QBO Signal in Total Ozone Over the Tibet, Climatic and Environmental Research, 6, 416–424, 2001.

Jia, S., Xu, X., Lin, W., Wang, Y., He, X., and Zhang, H.: Increased mixing ratio of surface ozone by nighttime convection process over the North China Plain, Journal of Applied Meteorological Science, 26, 280–290, 2015.

Koumoutsaris, S., Bey, I., Generoso, S., and Thouret, V.: Influence of El Niño–Southern Oscillation on the interannual variability of tropospheric ozone in the northern midlatitudes, J. Geophys. Res.-Atmos., 113, D19301, https://doi.org/10.1029/2007JD009753, 2008.

Kurokawa, J., Ohara, T., Morikawa, T., Hanayama, S., Janssens-Maenhout, G., Fukui, T., Kawashima, K., and Akimoto, H.: Emissions of air pollutants and greenhouse gases over Asian regions during 2000–2008: Regional Emission inventory in ASia (REAS) version 2, Atmos. Chem. Phys., 13, 11019–11058, https://doi.org/10.5194/acp-13-11019-2013, 2013.

Kwan, K. F. and Samah, A. A.: A conceptual model relating the quasi-biennial oscillation and the tropospheric biennial oscillation, Int. J. Climatol., 23, 347–362, https://doi.org/10.1002/joc.876, 2003.

Lal, S., Venkataramani, S., Chandra, N., Cooper, O. R., Brioude, J., and Naja, M.: Transport effects on the vertical distribution of tropospheric ozone over western India, J. Geophys. Res.-Atmos., 119, 10012–10026, https://doi.org/10.1002/2014JD021854, 2014.

Langford, A. O.: Stratosphere-troposphere exchange at the subtropical jet: Contribution to the tropospheric ozone budget at midlatitudes, Geophys. Res. Lett., 26, 2449–2452, https://doi.org/10.1029/1999GL900556, 1999.

Langford, A. O., Aikin, K. C., Eubank, C. S., and Williams, E. J.: Stratospheric contribution to high surface ozone in Colorado during springtime, Geophys. Res. Lett., 36, L12801, https://doi.org/10.1029/2009GL038367, 2009.

Langford, A. O., Senff, C. J., Alvarez Ii, R. J., Brioude, J., Cooper, O. R., Holloway, J. S., Lin, M. Y., Marchbanks, R. D., Pierce, R. B., Sandberg, S. P., Weickmann, A. M., and Williams, E. J.: An overview of the 2013 Las Vegas Ozone Study (LVOS): Impact of stratospheric intrusions and long-range transport on surface air quality, Atmos. Environ., 109, 305–322, https://doi.org/10.1016/j.atmosenv.2014.08.040, 2015.

Lee, H. N., Tositti, L., Zheng, X., and Bonasoni, P.: Analyses and comparisons of variations of ^{7}Be, ^{210}Pb, and ^{7}Be/^{210}Pb with ozone observations at two Global Atmosphere Watch stations from high mountains, J. Geophys. Res.-Atmos., 112, D05303, https://doi.org/10.1029/2006JD007421, 2007.

Lefohn, A. S., Wernli, H., Shadwick, D., Oltmans, S. J., and Shapiro, M.: Quantifying the importance of stratospheric-tropospheric transport on surface ozone concentrations at high- and low-elevation monitoring sites in the United States, Atmos. Environ., 62, 646–656, https://doi.org/10.1016/j.atmosenv.2012.09.004, 2012.

Li, J. and Zeng, Q.: A unified monsoon index, Geophys. Res. Lett., 29, 115.111–115.114, https://doi.org/10.1029/2001GL013874, 2002.

Liang, M.-C., Tang, J., Chan, C.-Y., Zheng, X. D., and Yung, Y. L.: Signature of stratospheric air at the Tibetan Plateau, Geophys. Res. Lett., 35, L20816, https://doi.org/10.1029/2008GL035246, 2008.

Lin, M., Fiore, A. M., Cooper, O. R., Horowitz, L. W., Langford, A. O., Levy, H., Johnson, B. J., Naik, V., Oltmans, S. J., and Senff, C. J.: Springtime high surface ozone events over the western United States: Quantifying the role of stratospheric intrusions, J. Geophys. Res.-Atmos., 117, D00V22, https://doi.org/10.1029/2012JD018151, 2012a.

Lin, M., Fiore, A. M., Horowitz, L. W., Cooper, O. R., Naik, V., Holloway, J., Johnson, B. J., Middlebrook, A. M., Oltmans, S. J., Pollack, I. B., Ryerson, T. B., Warner, J. X., Wiedinmyer, C., Wilson, J., and Wyman, B.: Transport of Asian ozone pollution into surface air over the western United States in spring, J. Geophys. Res.-Atmos., 117, D00V07, https://doi.org/10.1029/2011JD016961, 2012b.

Lin, M., Horowitz, L. W., Oltmans, S. J., Fiore, A. M., and Fan, S.: Tropospheric ozone trends at Mauna Loa Observatory tied to decadal climate variability, Nat. Geosci., 7, 136–143, https://doi.org/10.1038/ngeo2066, 2014.

Lin, M., Fiore, A. M., Horowitz, L. W., Langford, A. O., Oltmans, S. J., Tarasick, D., and Rieder, H. E.: Climate variability modulates western US ozone air quality in spring via deep stratospheric intrusions, Nat. Commun., 6, 7105, https://doi.org/10.1038/ncomms8105, 2015a.

Lin, M., Horowitz, L. W., Cooper, O. R., Tarasick, D., Conley, S., Iraci, L. T., Johnson, B., Leblanc, T., Petropavlovskikh, I., and Yates, E. L.: Revisiting the evidence of increasing springtime ozone mixing ratios in the free troposphere over western North America, Geophys. Res. Lett., 8719–8728, https://doi.org/10.1002/2015GL065311, 2015b.

Lin, M., Horowitz, L. W., Payton, R., Fiore, A. M., and Tonnesen, G.: US surface ozone trends and extremes from 1980 to 2014: quantifying the roles of rising Asian emissions, domestic controls, wildfires, and climate, Atmos. Chem. Phys., 17, 2943–2970, https://doi.org/10.5194/acp-17-2943-2017, 2017.

Liu, G., Liu, J., Tarasick, D. W., Fioletov, V. E., Jin, J. J., Moeini, O., Liu, X., Sioris, C. E., and Osman, M.: A global tropospheric ozone climatology from trajectory-mapped ozone soundings, Atmos. Chem. Phys., 13, 10659–10675, https://doi.org/10.5194/acp-13-10659-2013, 2013.

Liu, H., Jacob, D. J., Chan, L. Y., Oltmans, S. J., Bey, I., Yantosca, R. M., Harris, J. M., Duncan, B. N., and Martin, R. V.: Sources of tropospheric ozone along the Asian Pacific Rim: An analysis of ozonesonde observations, J. Geophys. Res.-Atmos., 107, 4573, https://doi.org/10.1029/2001JD002005, 2002.

Liu, J. J., Jones, D. B. A., Worden, J. R., Noone, D., Parrington, M., and Kar, J.: Analysis of the summertime buildup of tropospheric ozone abundances over the Middle East and North Africa as observed by the Tropospheric Emission Spectrometer instrument, J. Geophys. Res.-Atmos., 114, D05304, https://doi.org/10.1029/2008JD010993, 2009.

Liu, J. J., Jones, D. B. A., Zhang, S., and Kar, J.: Influence of interannual variations in transport on summertime abundances of ozone over the Middle East, J. Geophys. Res.-Atmos., 116, D20310, https://doi.org/10.1029/2011JD016188, 2011.

Lucey, D., Hadjiiski, L., Hopke, P. K., Scudlark, J. R., and Church, T.: Identification of sources of pollutants in precipitation measured at the mid-Atlantic US coast using potential source contribution function (PSCF), Atmos. Environ., 35, 3979–3986, https://doi.org/10.1016/s1352-2310(01)00185-6, 2001.

Ma, J., Tang, J., Zhou, X., and Zhang, X.: Estimates of the Chemical Budget for Ozone at Waliguan Observatory, J. Atmos. Chem., 41, 21–48, https://doi.org/10.1023/A:1013892308983, 2002.

Ma, J., Zheng, X., and Xu, X.: Comment on "Why does surface ozone peak in summertime at Waliguan?" by Bin Zhu et al., Geophys. Res. Lett., 32, L01805, https://doi.org/10.1029/2004GL021683, 2005.

Ma, J., Lin, W. L., Zheng, X. D., Xu, X. B., Li, Z., and Yang, L. L.: Influence of air mass downward transport on the variability of surface ozone at Xianggelila Regional Atmosphere Background Station, southwest China, Atmos. Chem. Phys., 14, 5311–5325, https://doi.org/10.5194/acp-14-5311-2014, 2014.

Ma, Z., Xu, J., Quan, W., Zhang, Z., Lin, W., and Xu, X.: Significant increase of surface ozone at a rural site, north of eastern China, Atmos. Chem. Phys., 16, 3969–3977, https://doi.org/10.5194/acp-16-3969-2016, 2016.

Maycock, A. C., Matthes, K., Tegtmeier, S., Thiéblemont, R., and Hood, L.: The representation of solar cycle signals in stratospheric ozone – Part 1: A comparison of recently updated satellite observations, Atmos. Chem. Phys., 16, 10021–10043, https://doi.org/10.5194/acp-16-10021-2016, 2016.

Ningombam, S. S.: Variability of sunspot cycle QBO and total ozone over high altitude western Himalayan regions, J. Atmos. Sol.-Terr. Phy., 73, 2305–2313, https://doi.org/10.1016/j.jastp.2011.06.015, 2011.

Oman, L. D., Douglass, A. R., Ziemke, J. R., Rodriguez, J. M., Waugh, D. W., and Nielsen, J. E.: The ozone response to ENSO in Aura satellite measurements and a chemistry-climate simulation, J. Geophys. Res.-Atmos., 118, 965–976, https://doi.org/10.1029/2012JD018546, 2013.

Sioris, C. E., McLinden, C. A., Fioletov, V. E., Adams, C., Zawodny, J. M., Bourassa, A. E., Roth, C. Z., and Degenstein, D. A.: Trend and variability in ozone in the tropical lower stratosphere over 2.5 solar cycles observed by

SAGE II and OSIRIS, Atmos. Chem. Phys., 14, 3479–3496, https://doi.org/10.5194/acp-14-3479-2014, 2014.

Škerlak, B., Sprenger, M., and Wernli, H.: A global climatology of stratosphere–troposphere exchange using the ERA-Interim data set from 1979 to 2011, Atmos. Chem. Phys., 14, 913–937, https://doi.org/10.5194/acp-14-913-2014, 2014.

Sprenger, M. and Wernli, H.: A northern hemispheric climatology of cross-tropopause exchange for the ERA15 time period (1979–1993), J. Geophys. Res.-Atmos., 108, 8521, https://doi.org/10.1029/2002JD002636, 2003.

Stohl, A., Spichtinger-Rakowsky, N., Bonasoni, P., Feldmann, H., Memmesheimer, M., Scheel, H. E., Trickl, T., Hübener, S., Ringer, W., and Mandl, M.: The influence of stratospheric intrusions on alpine ozone concentrations, Atmos. Environ., 34, 1323–1354, https://doi.org/10.1016/S1352-2310(99)00320-9, 2000.

Sun, L., Xue, L., Wang, T., Gao, J., Ding, A., Cooper, O. R., Lin, M., Xu, P., Wang, Z., Wang, X., Wen, L., Zhu, Y., Chen, T., Yang, L., Wang, Y., Chen, J., and Wang, W.: Significant increase of summertime ozone at Mount Tai in Central Eastern China, Atmos. Chem. Phys., 16, 10637–10650, https://doi.org/10.5194/acp-16-10637-2016, 2016.

Tang, Q., Prather, M. J., and Hsu, J.: Stratosphere-troposphere exchange ozone flux related to deep convection, Geophys. Res. Lett., 38, L03806, https://doi.org/10.1029/2010gl046039, 2011.

van der A, R. J., Peters, D. H. M. U., Eskes, H., Boersma, K. F., Van Roozendael, M., De Smedt, I., and Kelder, H. M.: Detection of the trend and seasonal variation in tropospheric NO_2 over China, J. Geophys. Res.-Atmos., 111, D12317, https://doi.org/10.1029/2005JD006594, 2006.

Verstraeten, W. W., Neu, J. L., Williams, J. E., Bowman, K. W., Worden, J. R., and Boersma, K. F.: Rapid increases in tropospheric ozone production and export from China, Nat. Geosci., 8, 690–695, https://doi.org/10.1038/ngeo2493, 2015.

Voulgarakis, A., Hadjinicolaou, P., and Pyle, J. A.: Increases in global tropospheric ozone following an El Niño event: examining stratospheric ozone variability as a potential driver, Atmos. Sci. Lett., 12, 228–232, https://doi.org/10.1002/asl.318, 2011.

Wang, R., Xu, X., Jia, S., Ma, R., Ran, L., Deng, Z., Lin, W., Wang, Y., and Ma, Z.: Lower tropospheric distributions of O_3 and aerosol over Raoyang, a rural site in the North China Plain, Atmos. Chem. Phys., 17, 3891–3903, https://doi.org/10.5194/acp-17-3891-2017, 2017.

Wang, T., Ding, A., Gao, J., and Wu, W. S.: Strong ozone production in urban plumes from Beijing, China, Geophys. Res. Lett., 33, L21806, https://doi.org/10.1029/2006gl027689, 2006a.

Wang, T., Wong, H. L. A., Tang, J., Ding, A., Wu, W. S., and Zhang, X. C.: On the origin of surface ozone and reactive nitrogen observed at a remote mountain site in the northeastern Qinghai-Tibetan Plateau, western China, J. Geophys. Res.-Atmos., 111, D08303, https://doi.org/10.1029/2005JD006527, 2006b.

Wang, T., Wei, X. L., Ding, A. J., Poon, C. N., Lam, K. S., Li, Y. S., Chan, L. Y., and Anson, M.: Increasing surface ozone concentrations in the background atmosphere of Southern China, 1994–2007, Atmos. Chem. Phys., 9, 6217–6227, https://doi.org/10.5194/acp-9-6217-2009, 2009.

Wang, Y., Konopka, P., Liu, Y., Chen, H., Müller, R., Plöger, F., Riese, M., Cai, Z., and Lü, D.: Tropospheric ozone trend over Beijing from 2002–2010: ozonesonde measurements and modeling analysis, Atmos. Chem. Phys., 12, 8389–8399, https://doi.org/10.5194/acp-12-8389-2012, 2012.

Xu, W., Lin, W., Xu, X., Tang, J., Huang, J., Wu, H., and Zhang, X.: Long-term trends of surface ozone and its influencing factors at the Mt Waliguan GAW station, China – Part 1: Overall trends and characteristics, Atmos. Chem. Phys., 16, 6191–6205, https://doi.org/10.5194/acp-16-6191-2016, 2016.

Xu, X., Lin, W., Wang, T., Yan, P., Tang, J., Meng, Z., and Wang, Y.: Long-term trend of surface ozone at a regional background station in eastern China 1991–2006: enhanced variability, Atmos. Chem. Phys., 8, 2595–2607, https://doi.org/10.5194/acp-8-2595-2008, 2008.

Xue, L. K., Wang, T., Zhang, J. M., Zhang, X. C., Deliger, Poon, C. N., Ding, A. J., Zhou, X. H., Wu, W. S., Tang, J., Zhang, Q. Z., and Wang, W. X.: Source of surface ozone and reactive nitrogen speciation at Mount Waliguan in western China: New insights from the 2006 summer study, J. Geophys. Res., 116, D07306, https://doi.org/10.1029/2010jd014735, 2011.

Yang, Y., Liao, H., and Li, J.: Impacts of the East Asian summer monsoon on interannual variations of summertime surface-layer ozone concentrations over China, Atmos. Chem. Phys., 14, 6867–6879, https://doi.org/10.5194/acp-14-6867-2014, 2014.

Zeng, G. and Pyle, J. A.: Influence of El Niño Southern Oscillation on stratosphere/troposphere exchange and the global tropospheric ozone budget, Geophys. Res. Lett., 32, L01814, https://doi.org/10.1029/2004GL021353, 2005.

Zeng, Y. and Hopke, P. K.: A studyof the sources of acid precipitation in Ontario, Canada, Atmos. Environ., 23, 1499–1509, 1989.

Zhang, F., Zhou, L. X., Novelli, P. C., Worthy, D. E. J., Zellweger, C., Klausen, J., Ernst, M., Steinbacher, M., Cai, Y. X., Xu, L., Fang, S. X., and Yao, B.: Evaluation of in situ measurements of atmospheric carbon monoxide at Mount Waliguan, China, Atmos. Chem. Phys., 11, 5195–5206, https://doi.org/10.5194/acp-11-5195-2011, 2011.

Zheng, X. D., Shen, C. D., Wan, G. J., Liu, K. X., Tang, J., and Xu, X. B.: $\sim (10)Be/\sim 7Be$ implies the contribution of stratosphere-troposphere transport to the winter-spring surface O_3 variation observed on the Tibetan Plateau, Chinese Sci. Bull., 56, 84–88, 2011.

Zhou, L., Hopke, P. K., and Liu, W.: Comparison of two trajectory based models for locating particle sources for two rural New York sites, Atmos. Environ., 38, 1955–1963, https://doi.org/10.1016/j.atmosenv.2003.12.034, 2004.

Zhu, B., Akimoto, H., Wang, Z., Sudo, K., Tang, J., and Uno, I.: Why does surface ozone peak in summertime at Waliguan?, Geophys. Res. Lett., 31, L17104, https://doi.org/10.1029/2004GL020609, 2004.

Ziemke, J. R., Chandra, S., and Bhartia, P. K.: A 25-year data record of atmospheric ozone in the Pacific from Total Ozone Mapping Spectrometer (TOMS) cloud slicing: Implications for ozone trends in the stratosphere and troposphere, J. Geophys. Res.-Atmos., 110, D15105, https://doi.org/10.1029/2004JD005687, 2005.

Ziemke, J. R., Chandra, S., Oman, L. D., and Bhartia, P. K.: A new ENSO index derived from satellite measurements of column ozone, Atmos. Chem. Phys., 10, 3711–3721, https://doi.org/10.5194/acp-10-3711-2010, 2010.

Zou, H., Ji, C. P., Zhou, L. B., Wang, W., and Jiang, Y. X.: ENSO
   Signal in Total Ozone over Tibet, Climatic and Environmental
   Research, 6, 267–272, 2001.